

**VAPOR-PHASE CATALYTIC UPGRADING OF BIOMASS PYROLYSIS
PRODUCTS THROUGH ALDOL CONDENSATION AND
HYDRODEOXYGENATION FOR THE FORMATION OF FUEL-RANGE
HYDROCARBONS**

by

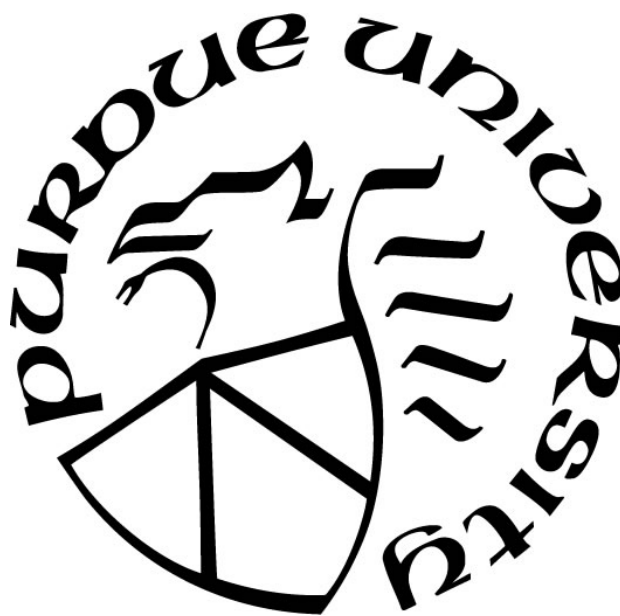
Richard Caulkins

A Thesis

Submitted to the Faculty of Purdue University

In Partial Fulfillment of the Requirements for the degree of

Master of Science in Chemical Engineering



Davidson School of Chemical Engineering

West Lafayette, Indiana

December 2018

**THE PURDUE UNIVERSITY GRADUATE SCHOOL
STATEMENT OF COMMITTEE APPROVAL**

Dr. Fabio Ribeiro, Chair

Davidson School of Chemical Engineering

Dr. Rakesh Agrawal

Davidson School of Chemical Engineering

Dr. Jeffrey Miller

Davidson School of Chemical Engineering

Approved by:

Dr. John Morgan

Head of the Graduate Program

For my family and friends

ACKNOWLEDGMENTS

I would like to thank my family, and my parents in particular, without whose unwavering support in all my endeavors I would not be here. I would like to thank my advisor, Professor Fabio H. Ribeiro, and my other two committee members, Professor Rakesh Agrawal and Professor Jeffrey Miller. I would also like to thank Professor Hilikka Kenttämä and Professor W. Nicholas Delgass, who have provided excellent feedback on both the pyrolysis and catalysis experiments which are presented here. I would like to thank the members of the C3Bio group at Purdue both past and present whose work plays a vital role in the conclusions presented here. The mentoring of Dr. Harshavardhan Choudhari and Dr. John Degenstein was particularly invaluable. Ian Smith and Abhijit Talpade have provided vital feedback and suggestions which have helped move this project forward. Taufik Ridha and Emre Gencer have provided tremendous support to the catalytic efforts through their work in modeling a reaction network which will be able to select optimal reaction pathways for the production of liquid fuels. I would like to thank all of the members of the Purdue Catalysis Center who have not already been mentioned. This center has been a fruitful source of conversations and collaborations which have been extremely useful in advancing my understanding of catalysis. Finally, I would like to thank my funding source, the United States Department of Energy, Office of Science, Office of Basic Energy Sciences, through the Center for Direct Catalytic Conversion of Biomass to Biofuels (C3Bio), an Energy Frontier Research Center (award number DE-SC0000997).

TABLE OF CONTENTS

LIST OF TABLES	7
LIST OF FIGURES	8
LIST OF ABBREVIATIONS.....	11
ABSTRACT	12
1. INTRODUCTION	14
1.1 Production of Liquid Fuels through the H ₂ Bioil Process	14
1.2 Biomass Pyrolysis Product Distribution.....	15
1.3 Hydrodeoxygenation of Pyrolysis Vapors.....	16
1.4 Aldol Condensation	16
1.5 Aldol Condensation Mechanism	18
2. METHODS AND MATERIALS.....	21
2.1 Catalyst Preparation.....	21
2.2 Reactants.....	21
2.3 Pulsed Micro-reactor: Pyroprobe	22
2.4 Continuous Flow Fixed-bed Reactor.....	24
2.5 Group Contribution Method for Analysis of FID Peak Areas	25
3. RESULTS AND DISCUSSION.....	27
3.1 Aldol Condensation in the Pyroprobe Reactor.....	27
3.1.1 Aldol Condensation of Butanal in the Pyroprobe	28
3.1.2 Aldol Condensation and Hydrodeoxygenation of Glycolaldehyde.....	30
3.1.3 Aldol Condensation and Hydrodeoxygenation of Cellulose Pyrolysis Vapors	33
3.2 Aldol Condensation of Butanal in the Continuous-Flow Fixed Bed Reactor.....	35
3.2.1 Aldol Condensation of Butanal over Cu/TiO ₂	36
3.2.2 2% Cu/TiO ₂ Deactivation during Aldol Condensation of Butanal	41
3.2.3 Aldol Condensation of Butanal over TiO ₂	47
3.2.4 TiO ₂ Stability during Aldol Condensation of Butanal.....	51
3.3 Effects of feedstock on product carbon distribution.....	53
3.3.1 Pyrolysis plus HDO of Genetic Variants.....	53
3.3.2 Pyrolysis plus HDO of CDL Residue.....	55

4. CONCLUSIONS.....	59
APPENDIX A. DETAILED PRODUCT DISTRIBUTION FOR THE PYROLYSIS AND HDO OF POPLAR GENETIC VARIANTS	62
APPENDIX B. DETAILED PRODUCT DISTRIBUTION FOR THE PYROLYSIS AND HDO OF POPLAR CDL RESIDUE	66
REFERENCES	70

LIST OF TABLES

Table 1: Effective carbon number contributions for relevant functional groups for the estimation of FID response factors based on molecular structure	25
Table 2: Carbon selectivity to char during pyrolysis of wild type poplar and CDL residue from poplar	58

LIST OF FIGURES

Figure 1: Product carbon selectivity at 100% conversion from the aldol condensation of butanal over 2% Cu/TiO ₂ at 300°C and 30 psi H ₂ , with >80% carbon balance.....	29
Figure 2: Product carbon yields at 100% conversion from the aldol condensation and sequential hydrodeoxygenation of glycolaldehyde over 2% Cu/TiO ₂ followed by 5% PtMo/MWCNTs at 300°C and 40 psi H ₂ , with 60% carbon balance, or 300 psi, with 90% carbon balance.....	30
Figure 3: Carbon selectivity to linear versus nonlinear hydrocarbon products from the aldol condensation and hydrodeoxygenation of glycolaldehyde.....	32
Figure 4: Product carbon distribution from the aldol condensation and sequential hydrodeoxygenation of cellulose over Cu/TiO ₂ and PtMo/MWCNTs at 300°C and 3 bar H ₂	33
Figure 5: Product carbon distribution from the aldol condensation and sequential hydrodeoxygenation of cellulose over Cu/TiO ₂ and PtMo/MWCNTs at 300°C and 40 psi H ₂ or 300 psi H ₂	35
Figure 6: Structures for observed minor C ₈ products. At the top from left to right: 4-methylheptanone and butyl ester butanoic acid. At the bottom: 2-ethyl-hexanoic acid...38	38
Figure 7: Selectivity to products by number of aldol condensations as a function of conversion over 2% Cu/TiO ₂ at 300°C and 1 bar H ₂	40
Figure 8: Carbon selectivity to the major observed products as a function of conversion over the 2% Cu/TiO ₂ catalyst at 300°C and 1 bar H ₂	40
Figure 9: Expanded view of carbon selectivity to the minor products (carbon selectivity < 10%) as a function of conversion over 2% Cu/TiO ₂ at 300°C and 1 bar H ₂	41
Figure 10: Deactivation of 2% Cu/TiO ₂ at moderate conversion	42
Figure 11: Deactivation behavior of 2% Cu/TiO ₂ at moderate conversion: dynamic product carbon distribution.....	43
Figure 12: Stability of Cu/TiO ₂ at low conversion	44
Figure 13: Stability of 2% Cu/TiO ₂ over 16 hours.....	45
Figure 14: Stability of 2% Cu/TiO ₂ over 16 hours: dynamic product distribution.....	46
Figure 15: Effects of overnight hydrogen flow on 2% Cu/TiO ₂	47

Figure 16: Product carbon distribution from aldol condensation of butanal over TiO ₂ at 300°C and 1 bar H ₂	48
Figure 17: Product carbon distribution for major products over TiO ₂ at 300°C and 1 bar H ₂	48
Figure 18: MS EI fragmentation pattern for the major C ₁₂ product from aldol condensation of butanal over TiO ₂	50
Figure 19: MS EI fragmentation pattern for the major C ₁₂ product from aldol condensation of butanal over 2% Cu/TiO ₂	50
Figure 20: Stability of TiO ₂ at moderate to low conversion	51
Figure 21: Stability of TiO ₂ at moderate to low conversions: carbon selectivity to the major product, 2-ethyl-hexenal	52
Figure 22: Stability of TiO ₂ at moderate to low conversions: carbon selectivity to minor products	52
Figure 23: Monomers of lignin. p-coumaryl alcohol forms H units, coniferyl alcohol forms G units, and sinapyl alcohol forms S units.	53
Figure 24: Carbon distribution by carbon number for HDO of poplar and poplar genetic variants over 5% PtMo/MWCNTs at 300°C and 20.4 bar H ₂	54
Figure 25: Product distribution by carbon number for HDO of wild type poplar, CDL residue from poplar, and cellulose over 5% PtMo/MWCNTs at 300°C and 20.4 bar H ₂	55
Figure 26: Carbon selectivity to specific C ₆ products for HDO of poplar and CDL residue from poplar at 300°C and 20.4 bar H ₂	56
Figure 27: Carbon selectivity to specific C ₇ products for HDO of poplar and CDL residue from poplar at 300°C and 20.4 bar H ₂	57
Figure 28: Carbon selectivity to specific C ₄ products for HDO of poplar genetic variants at 300°C and 20.4 bar H ₂	62
Figure 29: Carbon selectivity to specific C ₅ products for HDO of poplar genetic variants at 300°C and 20.4 bar H ₂	63
Figure 30: Carbon selectivity to specific C ₆ products for HDO of poplar genetic variants at 300°C and 20.4 bar H ₂	63
Figure 31: Carbon selectivity to specific C ₇ products for HDO of poplar genetic variants at 300°C and 20.4 bar H ₂	64

Figure 32: Carbon selectivity to specific C8 products for HDO of poplar genetic variants at 300°C and 20.4 bar H2.....	65
Figure 33: Carbon selectivity to specific C9 products for HDO of poplar genetic variants at 300°C and 20.4 bar H2.....	65
Figure 34: Carbon selectivity to specific C4 products for HDO of poplar and CDL residue from poplar at 300°C and 20.4 bar H2.....	66
Figure 35: Carbon selectivity to specific C5 products for HDO of poplar and CDL residue from poplar at 300°C and 20.4 bar H2.....	67
Figure 36: Carbon selectivity to specific C6 products for HDO of poplar and CDL residue from poplar at 300°C and 20.4 bar H2.....	67
Figure 37: Carbon selectivity to specific C7 products for HDO of poplar and CDL residue from poplar at 300°C and 20.4 bar H2.....	68
Figure 38: Carbon selectivity to specific C\8 products for HDO of poplar and CDL residue from poplar at 300°C and 20.4 bar H2.....	68
Figure 39: Carbon selectivity to specific C9 products for HDO of poplar and CDL residue from poplar at 300°C and 20.4 bar H2.....	69

LIST OF ABBREVIATIONS

MWCNTs – Multiwalled carbon nanotubes

HDO – hydrodeoxygenation

GC – Gas Chromatograph

CDL – Catalytic depolymerization of lignin, a process developed by Abu-Omar and coworkers

MSD – Mass spectrometer detector

FID – Flame Ionization Detector

TCD – Thermal Conductivity Detector

ECN – Effective Carbon Number

ABSTRACT

Author: Caulkins, Richard, S. MSCHE

Institution: Purdue University

Degree Received: December 2018

Title: Vapor-Phase Catalytic Upgrading of Biomass Pyrolysis Products through Aldol

Condensation and Hydrodeoxygenation for the Formation of Fuel-Range Hydrocarbons

Committee Chair: Fabio Ribeiro

Biomass-derived fuels have long been considered as a possible replacement for traditional liquid fuels derived from petroleum. However, biomass as a feedstock requires significant refinement prior to application as a liquid fuel. The H₂Bioil process has previously been proposed in which biomass is pyrolyzed and the resulting vapors are passed over a catalyst bed for upgrading to hydrocarbon products in a hydrogen environment [1]. A PtMo catalyst has been developed for the complete hydrodeoxygenation (HDO) of biomass pyrolysis vapors to hydrocarbons [2]. However, the product hydrocarbons contain a large fraction of molecules smaller than C₄ which would not be suitable as liquid fuels. In fast hydrolysis of poplar followed by hydrodeoxygenation over a PtMo/MWCNT catalyst at 25 bar H₂ and 300°C, only 32.1% of carbon is captured in C₄ – C₈ products; 21.7% of carbon is captured in C₁ – C₃ hydrocarbons [2]. Here, approaches are examined to increase selectivity of H₂Bioil to desired products. Aldol condensation catalysts could be used prior to the HDO catalyst in order to increase the carbon number of products. These products would then be hydrodeoxygenated to hydrocarbons of greater average carbon number than with an HDO catalyst alone. Application of a 2% Cu/TiO₂ catalyst to a classic aldehyde model compound, butanal, shows high selectivity towards aldol condensation products at low H₂ pressures. In more complex systems which more closely resemble biomass pyrolysis vapors, this catalyst also shows significant yields to aldol condensation products, but substantial carbon losses presumed to be due to coke formation are observed. Both glycolaldehyde, a significant product of biomass pyrolysis, and cellulose, a component polymer of biomass, have been pyrolyzed and passed through aldol condensation followed by hydrodeoxygenation in a pulsed fixed-bed microreactor. Glycolaldehyde aldol condensation resulted in the formation of products in the C₂-C₉ range, while the major aldol condensation products observed from cellulose were C₇ and C₈ products. Carbon losses in glycolaldehyde aldol condensation were reduced under operation at increased hydrogen partial

pressures, supporting the hypothesis that increasing selectivity to hydrogenation products can reduce coke formation from primary aldol condensation products.

The use of feeds which have undergone genetic modification and/or pretreatment by other catalytic processes may also lead to improvements in overall product selectivity. The influence of genetic modifications to poplar lignin on the pyrolysis plus HDO process are investigated, and it is found that these materials have no effect on the final product distribution. The product distribution from a poplar sample which has had lignin catalytically removed is also examined, with the conclusion that the product distribution strongly resembles that of cellulose, however the lignin-removed sample shows high selectivity towards char which is not seen from cellulose.

1. INTRODUCTION

1.1 Production of Liquid Fuels through the H₂Bioil Process

Reducing dependence on fossil fuels through the development of alternative energy sources is desirable for reducing dependence on petroleum imports as well as for reducing carbon emissions. Although many strategies have been proposed for the production of electricity from renewable energy, the transportation sector remains reliant on petroleum-based fuels. The US is projected to consume 19.6 million barrels per day of crude oil compared to the production of 10.6 million barrels per day in 2020, with a net import of crude oil expected to be needed through 2040 [3]. Although natural gas, solar, wind, and nuclear power offer relatively clean sources of electricity, none of these are suitable for use as transportation fuels. Liquid fuels are currently safer and cheaper to store and use in vehicles than many proposed alternative fuel sources, such as hydrogen [4]. In addition, the infrastructure for distribution of liquid fuels is already in place, while a gas-based distribution system would require extensive development. Gasification could be used to transform natural gas or biomass into liquid fuels, however gasification followed by Fischer-Tropsch synthesis requires excessive amounts of hydrogen [1,5]. Given these limitations of renewable energy and the advantages of using liquid fuels, the H₂Bioil process was proposed by Agrawal and Singh to use solar energy to produce hydrogen, which can then be used in much smaller quantities than in gasification and Fischer-Tropsch to perform reactions to transform biomass into liquid fuel [1]. As a solid, biomass has relatively low energy density due to the abundance of oxygen-containing functional groups in its component polymers cellulose, hemicellulose, and lignin. In H₂Bioil, biomass is pyrolyzed and hydrodeoxygenated in order to produce fuels with optimal hydrogen use [1]. A PtMo bimetallic catalyst has already been developed to perform hydrodeoxygenation, and its selectivity to hydrogenated or dehydrogenated products may be controlled by varying the hydrogen partial pressure. 37.1% of carbon from pyrolysis and HDO of poplar goes to C₄₊ products [2], and though different feedstocks will give variations in this number, a significant portion of the product distribution is lost to CO, CO₂, char, and C₁-C₃ hydrocarbon products. If C₄ through C₉ molecules are considered as being suitable for gasoline, then a significant portion of biomass pyrolysis vapors are unsuitable for liquid fuels. An additional reaction step to take advantage of the presence of

oxygen functional groups to lengthen carbon chain lengths would greatly increase the selectivity of the process to product molecules that are in the liquid fuel range.

Aldol condensation has been selected as the reaction of interest for increasing the average carbon number of H₂Bioil products molecules. The abundance of alcohol and aldehyde groups in the biomass pyrolysis product distribution means that there are many opportunities for aldol condensation to occur; as an example, glycolaldehyde makes up approximately 5-10% of the pyrolysis product distribution [6]. A glycolaldehyde molecule could undergo aldol condensation with another glycolaldehyde molecule, or with another carbonyl-containing product molecule such as furfural. Vapor-phase upgrading of glycolaldehyde to larger molecules is rarely studied in the literature. Furan production from glycolaldehyde over HZSM-5 was studied by Kim et. al. using a microreactor system, and products were analyzed by GCMS. Although furan products were observed, total conversion was less than 2% [7]. Studies at such low conversions do not give sufficient information as to the performance of the catalyst under realistic conditions, particularly since a key challenge in aldol condensation is coke formation due to multiple condensations taking place on the surface of a catalyst. Although aldol condensation is a well-studied reaction with applications in biomass, little work has been done to apply aldol condensation to pyrolysis products from intact biomass. The ultimate goal is to develop a catalyst and a set of reaction conditions that is capable of performing aldol condensation in series with the hydrodeoxygenation catalyst in a lab-scale reactor with improved selectivity towards fuel-range products with a biomass feed.

1.2 Biomass Pyrolysis Product Distribution

Biomass itself is composed primarily of three polymers: cellulose, hemicellulose, and lignin. Fast-pyrolysis results in the decomposition of these polymers into smaller molecules; this product stream can be analyzed directly by GC or it can be condensed into a bio-oil. Although the specific makeup of biomass is dependent on the source plant, cellulose and hemicellulose together compose 30-70% by weight of intact biomass [8]. Pyrolysis of cellulose gives high yields towards levoglucosan and its isomers of 50 wt% - 60 wt%; formic acid, glycolaldehyde, furan-based molecules, CO, and CO₂ account for approximately 25 wt% [9]. More specifically, during fast hydrolysis of cellulose at 480°C and 17 bar H₂ partial pressure and 10 bar He

partial pressure, selectivity towards glycolaldehyde in a collected liquid product has been reported as approximately 13% by weight [6]. During fast pyrolysis of cellulose at temperatures between 480°C and 500°C, selectivity towards glycolaldehyde has been reported as varying between 5% and 10% by weight [6,9,10]. Hemicellulose pyrolysis products are dominated by 50 wt% cumulative yield towards char, water, and CO and CO₂, but furan-based molecules, acetaldehyde, formic acid, acetic acid, and acetol account for the remainder of the product distribution [11]. Lignin pyrolysis gives 55 wt% yield to char, CO, and CO₂, with the remainder dominated by a variety of phenolic products, as would be expected from the linked aromatic units that compose lignin [12].

1.3 Hydrodeoxygenation of Pyrolysis Vapors

Hydrodeoxygenation is a key step in the treatment of pyrolysis vapors for the production of liquid fuels. Liquid fuels, composed primarily of hydrocarbons, have much higher energy densities than oxygen-rich biomass; poplar has an energy density of approximately 19 MJ/kg [1,13] compared to an energy density of approximately 46 MJ/kg for gasoline. A PtMo bimetallic catalyst has been reported for the hydrodeoxygenation of oxygenates found in biomass pyrolysis vapors [2,14]. A 5 wt% Pt 2.5 wt% Mo/MWCNTs catalyst has been reported to show complete hydrodeoxygenation of vapors from the fast hydrolysis of cellulose at 300°C under 25 bar H₂ pressure [6]. Similarly, in studies of hydrodeoxygenation of dihydroeugenol, a model compound for lignin, at 23.5 bar H₂ pressure, a PtMo catalyst has been shown to give high yield (>97%) to propylcyclohexane, with 0.7% yield towards propylbenzene [14,15]. These experiments have also been performed at 1 bar H₂, with the result of complete HDO but increased selectivity towards aromatic products over hydrogenated products compared to the high H₂ pressure work [16]. In this work, a 5% PtMo/MWCNTs catalyst is used for all HDO studies, in which Pt and Mo are present in a 1:1 ratio.

1.4 Aldol Condensation

Aldol condensation is a well-studied reaction with commercial applications. For example, 2-ethylhexanol is produced commercially by the aldol condensation of butyraldehyde catalyzed homogeneously by a basic solution to 2-ethylhexenal and subsequently hydrogenated over a

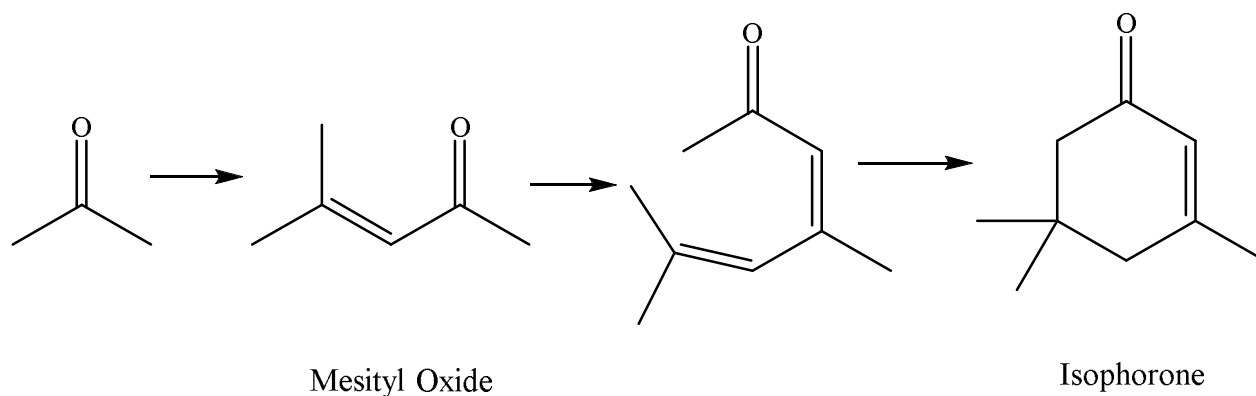
suitable solid catalyst [17]. In the field of heterogeneous catalysis, aldol condensation is most often performed over a metal oxide. MgO, ZrO₂, TiO₂, and the minerals hydroxyapatite (Ca₅(PO₄)₃(OH)) and hydrotalcite (Mg₆Al₂CO₃(OH)₁₆ · 4H₂O) are commonly studied aldol condensation catalysts [18–29]. Zeolite materials have also been studied for aldol condensation, typically with ion-exchanged alkali and alkaline earth metals ion [23,30,31]. Various oxides including ZnO, MgO, MoO₃, B₂O₃, and P₂O₅ have been deposited on ZSM-5 and Y-faujasite to investigate their effects on aldol condensation [32]. It was discovered that of these promoter oxides only B₂O₃ and P₂O₅, notable for their addition of further acidic sites to the zeolites, decreased the rate of aldol condensation, while the other oxides studied increased the rate of aldol condensation, likely through the addition of basic sites to the materials [32]. Strongly acidic sites in zeolites have been linked to the formation of coke during aldol condensation [30,32]. A Pd/ZrO₂ catalyst was studied by Gurbuz, Kunkes, and Dumesic. This catalyst was capable of performing aldol condensation and hydrogenation of C₅ ketones with total selectivity of approximately 60% to condensation products when operating at 66% conversion [29].

TiO₂ exists in several phases; the aldol condensation-relevant phases are anatase TiO₂ and rutile TiO₂, which differ in acid-base strength and in distance between pairs of Ti-O sites. Rutile TiO₂ deactivates much more quickly and has a much lower initial reaction rate than anatase TiO₂ during aldol condensation at the conditions of interest; the P25 TiO₂ is a mixture of approximately 75% anatase and 25% rutile, and behaves similarly to the anatase phase in aldol condensation [24].

Both acidic and basic sites play important roles in aldol condensation catalysis [24,25,32–35]. It has been found that alkali and alkaline earth metal ions added to MgO increased the number of basic sites on the catalyst according to the base strength of the oxide corresponding to a given promoter ion. Turnover rate was found to be proportional to the surface concentration of base sites [25].

Butyraldehyde and acetaldehyde are typical feeds of study for aldol condensation [18–20,32,36–39]. Aldol condensation of acetaldehyde leads to the formation of crotonaldehyde, while aldol condensation of butyraldehyde leads to the formation of 2-ethyl-hexenal. Ketones are also able to undergo aldol condensation, and acetone is commonly studied for this reaction. The condensation products from acetone are mesityl oxide and the double condensation product, shown in Reaction 1 [25,40]. It should be noted that the double condensation product undergoes

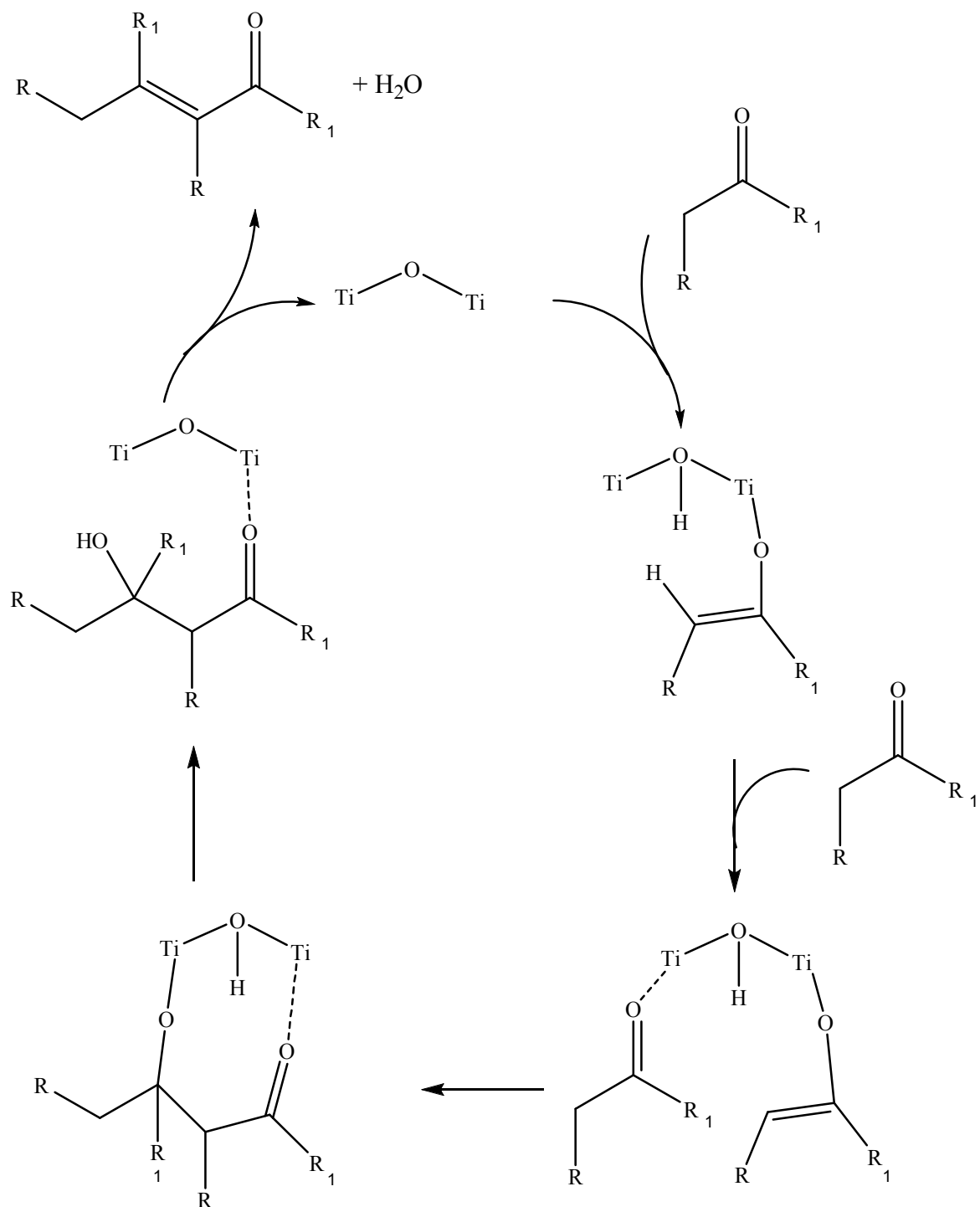
cyclization to form isophorone. Aldol condensation results in the formation of reactive functional groups, and following aldol condensation an aldehyde group remains; many secondary reactions are possible following a single condensation reaction, including a second condensation. This is demonstrated by the formation of isophorone from acetone.



Reaction 1: Aldol Condensation of Acetone

1.5 Aldol Condensation Mechanism

The mechanism of aldol condensation has been studied extensively, and is applicable to both aldehydes and ketones [22,24,29,37,41]. The mechanism for the aldol condensation of a generic aldehyde or ketone with a carbon backbone two carbons or longer is shown in Reaction 1, where R and R₁ are hydrogen atoms or alkyl groups. On TiO₂, aldol condensation begins with the adsorption of a carbonyl-containing molecule at the oxygen atom to the catalyst. A hydrogen atom from the α -C is abstracted by surface oxygen acting as a base, forming an enolate [42]. Lewis acid sites stabilize the transition state during enolate formation [24]. Additionally, DFT has shown that a methyl group at the α -C, as in propanal, leads to the formation of a more stable enolate as compared to if this R group is just a hydrogen atom, as in acetone [24]. Several studies have shown that enolate formation is the kinetically relevant step in this reaction [22,24], although it has also been suggested that product desorption could be kinetically relevant [20].



Reaction 2: Mechanism of Aldol Condensation over TiO_2 , as discussed by Wang, Goulas, and Iglesia [24]

Although adjacent acid-base Ti-O sites have been shown to be necessary for this reaction [24], it has been found to proceed with titanol sites in Ti/SiO₂, in which multiple butanal molecules may adsorb at a single Ti site [37]. DFT and experimental evidence showed that tetrahedrally coordinated Ti sites in Ti/SiO₂ are more active than hexacoordinated Ti sites [37]. Titania itself has also been studied. Rekoske and Barteau found that the anatase phase of titania was a highly selective catalyst for aldol condensation, but suffered from rapid deactivation due to the presence of large adsorbed molecules on the catalyst surface created during aldol condensation [19]. Recent work by Wang, Goulas, and Iglesia has shown that mixed Cu/SiO₂ and TiO₂ reduces catalyst deactivation through the hydrogenation of alkenal products to more stable alkanals following aldol condensation [24].

Although there are many examples in literature of aldol condensation of monofunctional aldehydes and ketones, there is much less work on molecules which contain both an aldehyde and an additional functional group that could play a role in the aldol condensation reaction. The bonding to the α -C could play an important role in stabilizing or detstabilizing the enolate intermediate, and so this work aims to study aldol condensation of both simple aldehydes and more complex feeds, with special focus on glycolaldehyde.

2. METHODS AND MATERIALS

2.1 Catalyst Preparation

Cu/TiO₂ was chosen as the catalyst for initial aldol condensation studies. TiO₂ is a well-known aldol condensation catalyst which deactivates very quickly [19]. Cu was chosen as a weak hydrogenation promoter [43]. The Cu/TiO₂ catalyst was synthesized through electrostatic adsorption of copper onto titania. Degussa P-25 TiO₂ (Aeroxide) was first densified by adding excess Millipore water to form a paste. This paste was dried at 120°C overnight and ground and sieved to a particle size of less than 250 μm. Copper (II) nitrate hydrate (99.999%, Alfa Aesar) was dissolved in Millipore water. Ammonium hydroxide was added to this solution until a deep blue solution was formed. TiO₂ and the copper solution were combined in Millipore water and filtered. The solid was dried at room temperature and at 120°C, and then calcined at 300°C for two hours. Following synthesis, the actual copper content of the catalyst was determined to be 2 wt% using a PerkinElmer 300 A Analyst atomic absorption spectrometer. The Cu/TiO₂ catalyst was reduced at 350°C for two hours prior to reaction in 30 mL/min He and 60 mL/min H₂. In order to avoid mass transfer limitations, the catalyst was sieved to a particle size between 125 μm and 250 μm.

The procedure used to synthesize PtMo/MWCNTs has been previously described [2]. It is synthesized through the incipient wetness impregnation of multiwalled carbon nanotubes (MWCNTs) (Cheap Tubes, Inc.) of Pt(NH₃)₄(NO₃)₂ (99.995%, Sigma Aldrich) and (NH₄)₆-Mo₇O₂₄·4H₂O (99.98%, Sigma Aldrich). Platinum and molybdenum are in a 1:1 ratio to form the 5% PtMo catalyst. The catalyst is dried overnight and calcined for 2 hours at 450°C. The PtMo/MWCNTs catalyst is reduced at 450°C for two hours prior to reaction. As with the Cu/TiO₂ catalyst, the PtMo catalyst was sieved to a particle size between 125 μm and 250 μm.

2.2 Reactants

Several model feeds were examined over the course of these experiments. Acetaldehyde (99.5%, Sigma Aldrich), butanal (99.0%, Sigma Aldrich), butanol (99.9%, Sigma Aldrich), 1,2-propanediol (99%, Sigma Aldrich), 1,3-propanediol (98%, Sigma Aldrich),

glycerol (99.5%, Sigma Aldrich), propylphenol (99%, Sigma Aldrich), and dihydroeugenol (99%, Sigma Aldrich) were examined as liquid feeds. Glycolaldehyde dimer (Sigma Aldrich) was examined as a 19 wt% in water solution. This dimer is known to decompose into monomer units at 100°C [7]. Levoglucosan and microcrystalline cellulose (50 µm, Sigma Aldrich) were pyrolyzed as solids.

2.3 Pulsed Micro-reactor: Pyroprobe

A pulse micro-reactor was used to study reactions of solid feeds as well as for preliminary studies of liquid model compounds. A CDS 5200 Pyroprobe was used to pyrolyze samples with the resulting vapors passed through a reactor. This unit contains a back pressure regulator capable of operating at temperatures of 300°C which was used to maintain pressures in the reactor between 2 bar and 20.4 bar. The unit was modified from the stock CDS 5200 pyroprobe such that following the reactor, product vapors were passed through the back pressure regulator and directly into a transfer line connected to the GC inlet, allowing for on-line analysis of reaction products without condensation of products. Liquid or solid samples are loaded inside of a ¼" quartz tube (CDS Analytical) and heated to the desired temperature at a rate of 1.00°C per millisecond. Nitrogen (99.995%, Inweld Corporation) was used to flush air from the quartz tube prior to pyrolysis in a hydrogen (99.999%, Praxair) or hydrogen plus helium (99.995%, Indiana Oxygen) environment. Biomass samples are pyrolyzed at 500°C; volatile liquid model compounds such as butanal are pyrolyzed at 100°C. Glycolaldehyde is loaded into the pyroprobe as a 19% solution in water by weight and pyrolyzed at 300°C. Solid samples of approximately 0.3 to 0.5 mg are coated onto the walls of the quartz tube. Liquid feeds of a single 1 µL droplet are deposited inside of the quartz tube using a 1 µL syringe. This minimizes temperature gradients inside the solid or liquid feed, so that the entire sample is assumed to be at the same temperature under pyrolysis conditions.

Pyrolysis vapors are swept into a fixed-bed reactor by a gas stream consisting of pure hydrogen or a mixture of helium and hydrogen. The catalyst is loaded into a stainless steel ¼" to ⅛" VCR male reducing union (Swagelok, SS-4-VCR-6-DM-2) which serves as the reactor for pyrolysis vapor upgrading. For HDO experiments, this reactor contains approximately 30 mg of 5% PtMo/MWCNTs with a layer of quartz wool both supporting the base of the catalyst and

covering the top of the catalyst. For aldol condensation experiments, the reactor contained an identical configuration, except that the catalyst was approximately 60 mg of 2% Cu/TiO₂. For dual-bed experiments with both the HDO and aldol condensation catalysts, 60 mg of Cu/TiO₂ catalyst were loaded above 30 mg of 5% PtMo/MWCNTs, separated by quartz wool and a stainless steel frit in order to prevent catalyst bed mixing. The reactor was kept at pressures between 30 psig for the lowest pressure experiments and 350 psig for the highest pressure experiments.

Following the reactor, product vapors were passed through a transfer line into an Agilent 7890A GC and 5975C MSD. Products were identified from the MSD using the NIST database. For experiments in which an HDO catalyst was applied, only hydrocarbon products were expected. Therefore, a J&W GS-GasPro column of length 6.2 m was used to separate products. For experiments in which a large amount of methane and ethane were produced, a CO₂ cryogenic valve assembly was used to introduce CO₂ (Liquid Withdraw, Indiana Oxygen) to the GC oven for the purpose of cooling it to temperatures below 35°C and improve separation of these light products. For experiments conducted without HDO catalyst, oxygenates were expected. For these experiments, an Agilent J&W DB-1701 column of length 60 m was used to separate products. A three-way splitter was used to divert a portion of the product stream to the MSD, with the remainder analyzed by an FID. Hydrogen (99.999%, Praxair) was used as the carrier gas.

Carbon balance in the pyroprobe experiments is calculated by determining the product carbon flow rates based on FID peak areas and by measuring the amount of char left following pyrolysis. Prior to pyrolysis, the mass of a solid loaded into the quartz tube is determined by massing the tube first without and then with sample loaded inside using a Mettler-Toledo XS205DU balance. Char masses were obtained by massing the quartz tube following pyrolysis. The carbon contents of intact cellulose and biomass and of the char produced from pyrolysis of intact biomass were determined by elemental analysis performed by Galbraith Laboratories (Knoxville, TN).

2.4 Continuous Flow Fixed-bed Reactor

A continuous flow fixed-bed reactor was used to study the catalyst at conversions less than 100%. A Chrom Tech Series III pump was used to feed butyraldehyde (99.0%, Sigma Aldrich) into the reactor at rates between 0.006 mL/min and 0.063 mL/min. The reactor inlet was heated to 180°C to ensure vaporization prior to contact with the catalyst bed. A gas stream consisting of ultra-high purity hydrogen (99.999%, Praxair), ultra-high purity helium (99.995%, Indiana Oxygen), and argon (99.995%, Indiana Oxygen) was fed into the reactor. Pressure inside the unit is maintained at 350 psi using a back pressure regulator.

The catalyst bed was kept at a temperature of 300.0°C ± 1.0°C during the reaction. Aldol condensation catalyst was loaded into the unit by packing a layer of mixed catalyst and quartz powder in between a top and bottom layer of quartz wool. Quartz powder was obtained by grinding quartz chips (Quartz Plus, Inc.) to particle sizes between 125 µm and 250 µm. Products were split to a condenser and to an Agilent 6890 GC.

Flow to the GC was automatically injected by a valve system in 30 minute intervals from a 3 mL sample loop and a 1 mL sample loop. Flow from the 3 mL sample loop was passed through a Supelco SPB-1 30 m long column to separate oxygenated products prior to entering an Agilent 3-way splitter which was used to split flow between an FID and an Agilent 5973N MSD. Products were identified from the MSD using the NIST database. Flow from the 1 mL sample loop was first passed through a Supelco 12718-U pre-column to remove heavy components from the product stream, then passed through a Supelco Carboxen 1000 packed column, which was used to separate light gases prior to detection by TCD. Helium (99.995%, Indiana Oxygen) was used as a carrier gas.

Reactions were allowed to continue for approximately eight hours until conversion ceased to drop by 1% over the course of multiple consecutive GC injections. Butanal flow was turned off and the catalyst was allowed to sit in 50 mL/min H₂ and 75 mL/min He at atmospheric pressure overnight prior to resumption of experiments the following day. Following stabilization of the catalyst over several days until a stable conversion was achieved, conversion was varied by varying the space velocity within the reactor while keeping the partial pressure of each component the same. This data was used to generate the selectivity versus conversion plots shown later.

2.5 Group Contribution Method for Analysis of FID Peak Areas

Flame ionization detectors give quantitative compositions of an inlet stream in the form of peak areas. Different components in the product stream have different combustion efficiencies, which are typically represented in the form of response factors. Although FID peak areas are not directly comparable, the choice of a reference compound and the normalization of all peak areas to that reference compound can be used to directly calculate a product distribution. These response factors can be determined through the injection of samples of varying but known composition containing the components of interest into the GC. However, it is not always practical to do so if these components are not readily available commercially. The response factor for a given component is related to its molecular structure. Therefore, if the molecular structure of a product molecule can be determined using MS, a response factor may be estimated. FID peak areas from the fixed bed reactor and pyroprobe experiments for the aldol condensation of butanal were analyzed using a group contribution method described by Scanlon and Willis [44]. In this method, an effective carbon number for a species is calculated based on its molecular structure. For the compounds of interest in this report, Table 1 shows the effective carbon number contribution used for each potentially relevant functional group, reproduced from the work by Scanlon and Willis [44].

Atom	Atomic Bonding	ECN contribution
C	Aliphatic or Aromatic	1
C	Olefinic	0.95
C	Carbonyl or Carboxyl	0
O	Ether	-1.0
O	Primary alcohol	-0.5
O	Secondary alcohol	-0.75

Table 1: Effective carbon number contributions for relevant functional groups for the estimation of FID response factors based on molecular structure

The effective carbon number (ECN) for a species is determined by the summation of effective carbon number contributions from each relevant atom. Based on the calculated effective carbon number, a response factor for the molecule may be calculated according to

$$\text{Molar Response Factor} = \frac{\text{ECN}_{\text{ref}}}{\text{ECN}_{\text{component}}}$$

ECN_{ref} is the effective carbon number of a reference compound, and $ECN_{component}$ is the effective carbon number of a compound of interest. For the work conducted here with butanal, butanal is the reference compound and ECN_{ref} is equal to 3. Corrected peak areas are calculated according to

$$Area_{corrected} = Area_{uncorrected} * \text{Molar Response Factor}$$

Butanal conversion is calculated by

$$\text{Conversion} = 1 - \frac{Area_{butanal}}{Area_{total,corrected}}$$

Product yields are calculated according to

$$\text{Yield} = \frac{Area_{corrected}}{\text{Conversion} * Area_{total,corrected}}$$

This technique was used to analyze GC data produced from the continuous-flow reactor. In all pyroprobe experiments in which oxygenates were detected, the ECN method was also used. However, when only hydrocarbon products were detected, such as with the sequential aldol condensation plus HDO experiments, a calibration had been developed for the GC relating peak area to product mass, allowing for the analysis of GC data without the ECN method.

3. RESULTS AND DISCUSSION

3.1 Aldol Condensation in the Pyroprobe Reactor

Preliminary work was done on the pyroprobe unit to confirm that the Cu/TiO₂ catalyst was active for aldol condensation, as well as to identify a model compound suitable for additional studies on the continuous-flow reactor. Butanal, glycolaldehyde, and cellulose were chosen for detailed studies in the pyroprobe system, but several additional compounds were studied for aldol condensation activity. Aldehydes were studied in order to find a model compound for extended studies in the continuous-flow reactor. Alcohols were examined in order to determine the ability of the Cu/TiO₂ catalyst to dehydrogenate the alcohol to an aldehyde to undergo subsequent aldol condensation. Alcohols equilibrate with the aldehyde form under the reaction conditions being studied here, so alcohols were also studied as aldol condensation feed streams since consumption of the equilibrated aldehyde product will drive formation of additional aldehyde [24]. Although the focus of the aldol condensation work is on cellulose and hemicellulose pyrolysis products, phenolic compounds were also examined as model compounds for lignin pyrolysis vapors to understand how these products may interact with Cu/TiO₂. Although aldol condensation of phenolic products is not expected due to the lack of α -H necessary for aldol condensation in benzaldehyde, some hydrodeoxygenation or hydrogenation could take place [45]. Among direct cellulose fast pyrolysis products, glycolaldehyde and levoglucosan were examined as components of interest due to their functionality and abundance in the pyrolysis product stream. Finally, cellulose fast pyrolysis vapor was studied directly as an aldol condensation feed.

Model aldehyde compounds were selected based on applicability to the system of interest and on practicality. For example, butyraldehyde was selected as a model compound for simple aldehydes due to its moderate vapor pressure at STP, allowing for the deposition of 1 μ L droplets in a quartz tube for study on the pyroprobe with minimal losses. Butyraldehyde additionally has a sufficiently low molecular weight as to allow for observation of multiple sequential aldol condensation products using GC/MS. A selected model compound would ideally be structurally similar to glycolaldehyde, the target molecule of interest in the biomass pyrolysis product distribution, but also readily available commercially for extended studies in the continuous flow

reactor. GC separation of aldol condensation was also critical to monomer selection, as dimers, trimers, and higher products formed from multiple aldol condensations must be efficiently separated. C₄, C₈, and C₁₂ molecules proved to be separable using a single capillary column, thus butyraldehyde was selected for extended studies in the continuous flow reactor.

Experiments conducted with butanol showed significant yields towards aldol condensation products. Butanal was observed in the absence of catalyst, and when butanol was passed over Cu/TiO₂, C₈ and C₁₂ hydrocarbons were observed. 1,2-propanediol, 1,3-propanediol, and glycerol were additionally examined in an effort to determine the effect of α -OH and β -OH groups on aldol condensation. No aldol condensation activity was observed with either of these feeds. Instead, various HDO products were observed in which one or more of the -OH groups were removed. Dihydroeugenol and propylphenol, chosen as model compounds for lignin, were also examined in the pyroprobe unit using the 2% Cu/TiO₂ catalyst. No aldol condensation products were observed from these feeds, however; instead, only hydrodeoxygenation and isomerization products were observed in low yield.

Although levoglucosan was vaporized and directly passed over the Cu/TiO₂ catalyst, a large number of products were observed. Clear structures for these products could not be identified, but they can be specified to be alkenes and cycloalkenes based on their m/z in EIMS spectra. Further work in which 5% PtMo/MWCNTs is applied to hydrodeoxygenate products would clarify the product distribution resulting from the reaction of levoglucosan, but initial results suggest that levoglucosan undergoes significant reaction in the Cu/TiO₂ system. Hydrocarbon products with C₄-C₈ could be identified, but a large number of low-abundance, heavier products were also observed that could not be clearly assigned a carbon number due to low signal/noise for these products in the MS spectra.

3.1.1 Aldol Condensation of Butanal in the Pyroprobe

Butanal was first examined in the pyroprobe in order to determine the ability of the Cu/TiO₂ to perform aldol condensation with a relatively simple aldehyde, the results of which can be seen in Figure 1. It showed 50% carbon selectivity towards butane, with the remaining 50% carbon going into aldol condensation-derived products in the C₈ and C₁₂ fraction.

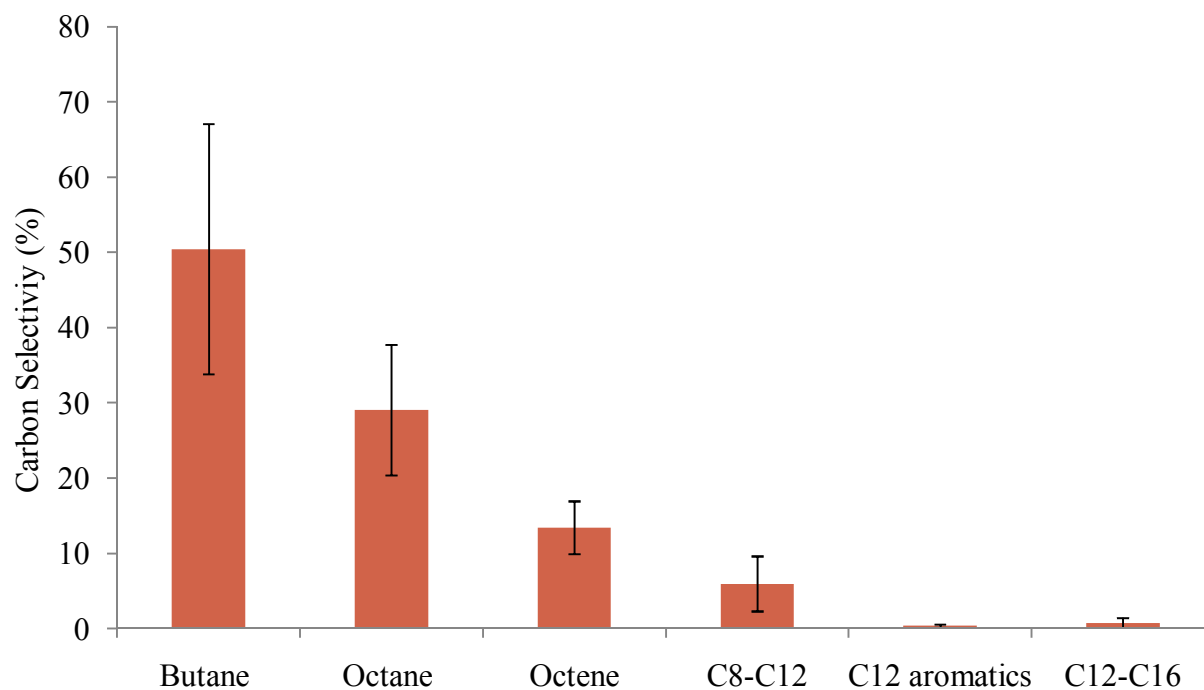


Figure 1: Product carbon selectivity at 100% conversion from the aldol condensation of butanal over 2% Cu/TiO₂ at 300°C and 30 psi H₂, with >80% carbon balance

It is interesting to note that in the pyroprobe only deoxygenated products were seen. As will be shown later, in contrast the continuous-flow reactor showed very low selectivity towards C₄ products, with approximately 5% of carbon going to predominantly butanol; butane and butene were present in < 1% abundance over the range of conversions examined. The high selectivity towards hydrodeoxygenated products observed in the pyroprobe may be due to non-steady state conditions present during the reaction that are fundamental to the design of the pyroprobe reactor. As described previously, the pyroprobe operates as a pulse-fed fixed bed reactor, with a continuous flow of hydrogen and/or helium. Under initial conditions, the surface of the catalyst should be saturated with hydrogen; when the pulse of aldol condensation reactant is fed into the system, it is exposed to a high surface hydrogen concentration, driving selectivity towards the hydrogen-consuming reactions hydrogenation and hydrodeoxygenation. This feature is not expected in a continuous-flow reactor, as the surface will have time to equilibrate with the feed of aldehyde reactant prior to data collection. In the case of butyraldehyde, this phenomenon would explain the observed high selectivity towards butane over aldol condensation products in the pyroprobe, in addition to the lack of oxygenated aldol condensation products. Results

obtained from the pyroprobe should therefore be considered as an upper limit on selectivity to hydrogenation and hydrodeoxygenation products.

3.1.2 Aldol Condensation and Hydrodeoxygenation of Glycolaldehyde

Aldol condensation alone of glycolaldehyde in the pyroprobe reactor resulted in the formation of a large number of alkenes in addition to oxygenated products that proved difficult to sufficiently separate for accurate quantification in the higher, C₈₊ carbon numbers. In order to enable accurate quantification of condensation products, a 5% PtMo/MWCNTs hydrodeoxygenation catalyst was loaded immediately after the 2% Cu/TiO₂ aldol condensation catalyst in order to simplify the product distribution such that only hydrocarbons were observed. As seen in Figure 2, aldol condensation of glycolaldehyde dimer solution showed 50% carbon selectivity among detected products towards ethane, the hydrodeoxygenation product, a similar selectivity to the reactant hydrodeoxygenation product butane in butyraldehyde experiments.

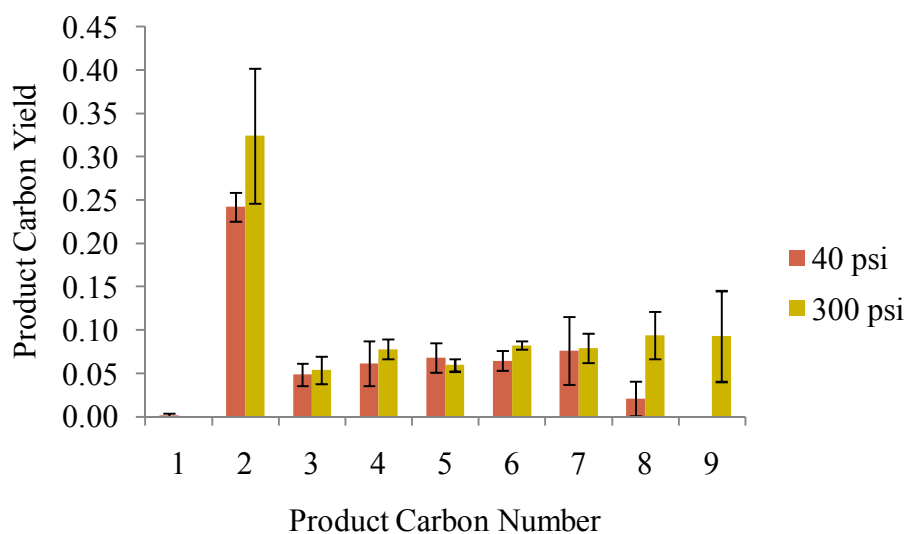


Figure 2: Product carbon yields at 100% conversion from the aldol condensation and sequential hydrodeoxygenation of glycolaldehyde over 2% Cu/TiO₂ followed by 5% PtMo/MWCNTs at 300°C and 40 psi H₂, with 60% carbon balance, or 300 psi, with 90% carbon balance

Analogous to the formation of butane from butyraldehyde in the pyroprobe reactor, high hydrogen surface coverage could explain the high yield to ethane. Higher molecular weight hydrocarbons were observed in high abundance. n-butane, n-hexane, and n-octane were observed as hydrodeoxygenation derivatives of direct aldol condensation products. Products of

non-aldol condensation side reactions were also observed. Multiple alkane products could be detected at carbon numbers C_4 and higher, indicating the presence of both linear and nonlinear alkanes; cycloalkanes were also observed in the C_{5+} range. The formation of these products indicates reorganization of the C-C backbone could be taking place via transalkylation or metathesis, or alternatively that additional carbonyl groups are generated in situ that provide additional aldol condensation sites within reactant molecules. C_3 , C_5 , C_7 , and C_9 products were also observed, indicative of C-C cleavage reactions. It is hypothesized that decarbonylation over the PtMo catalyst, resulting in the removal of terminal aldehydes as CO to leave behind molecules containing odd numbers of carbon atoms, could be responsible for the formation of these products. A reaction network for these products can be proposed, shown in Reaction 3 where products are mapped out to no more than two aldol condensations, where many possible products could form. The pathways shown can be extended to the case of additional sequential aldol condensation reactions. It is notable that due to the presence of the OH group at the α -C, the enal products can undergo tautomerization to form an isomer containing an additional carbonyl group. This additional carbonyl group can itself participate in additional aldol condensation reactions, ultimately resulting in the formation of branched hydrocarbons. Branched hydrocarbons are indeed observed in the glycolaldehyde aldol plus HDO system, as shown in Figure 3, but there is currently insufficient evidence to distinguish between these tautomerization-aldol condensation products and hydrocarbons formed through a transalkylation or metathesis reaction. The set of reactions proposed to take place in this system is shown in Reaction 3.

Substantial carbon losses were observed in this system: operation at 40 psi H_2 resulted in only 60% carbon recovery. It is hypothesized that these carbon losses are due to coke formation from larger aldol condensation products in the C_{10+} range. Operation at 300 psi H_2 in order to promote hydrogenation of aldol condensation products and suppress formation of these products supports this hypothesis, as carbon recovery was improved to 90% with significant increases in observed yields to C_8 and C_9 products. It is important to note that C_2 yields are increased, but not at the expense of C_{3+} products. This would indicate that at 300 psi H_2 , even under conditions of high surface hydrogen coverage, the carbonyl group is retained for aldol condensation, and is not instead reduced to an alcohol. Hydrogen partial pressure might be used to tune the product distribution in a continuous flow reactor, with 300 psi H_2 resulting in the observation of larger C_8

and C₉ products that were present only at extremely low abundances at 40 psi. This result is consistent with literature on coke formation on the surface of aldol condensation catalysts including TiO₂ after undergoing multiple aldol condensation reactions [19].

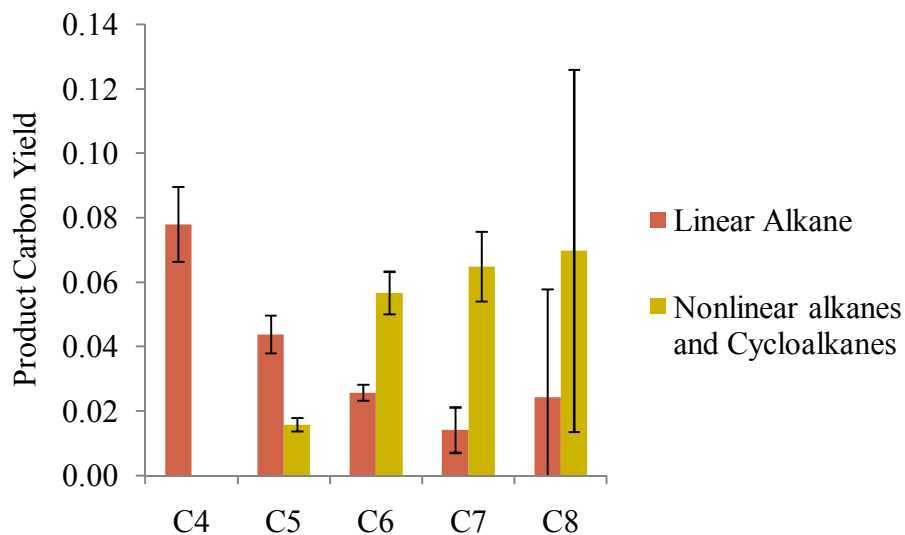
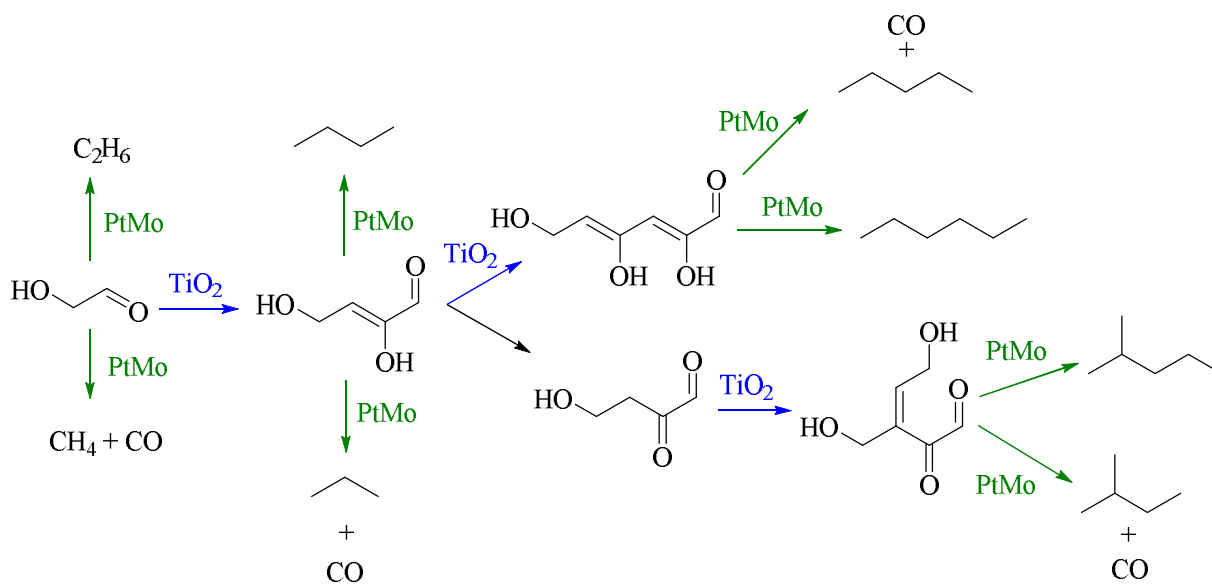


Figure 3: Carbon selectivity to linear versus nonlinear hydrocarbon products from the aldol condensation and hydrodeoxygenation of glycolaldehyde



Reaction 3: Reaction pathways observed for aldol condensation and hydrodeoxygenation of glycolaldehyde, including side reactions resulting in the formation of decarbonylated products

An alternative explanation for the abundance of C₂ products is the potential for esterification in place of aldol condensation. Esterification is a known side reaction competing with aldol condensation [24]. The continuous flow experiments with butanal show that selectivity to aldol condensation products is much greater than selectivity to esterification for the first condensation. However, further work would be required to study esterification in the pyroprobe, under non-steady state conditions. With the inclusion of a hydrodeoxygenation catalyst, any esterification products would be expected to form hydrocarbons with the same carbon number as the reactant, in this case glycolaldehyde.

3.1.3 Aldol Condensation and Hydrodeoxygenation of Cellulose Pyrolysis Vapors

Subjecting cellulose fast hydrolysis vapors to the aldol condensation plus hydrodeoxygenation catalyst system resulted in an increase in yields to C₇ and C₈ hydrocarbons at the expense of overall carbon balance. As with glycolaldehyde, a complex mixture of alkenes and oxygenates can be observed following direct aldol condensation of cellulose fast pyrolysis vapors. However, in the aldol condensation plus HDO system, the product distribution resolves into discrete carbon numbers with alkane and cycloalkane products.

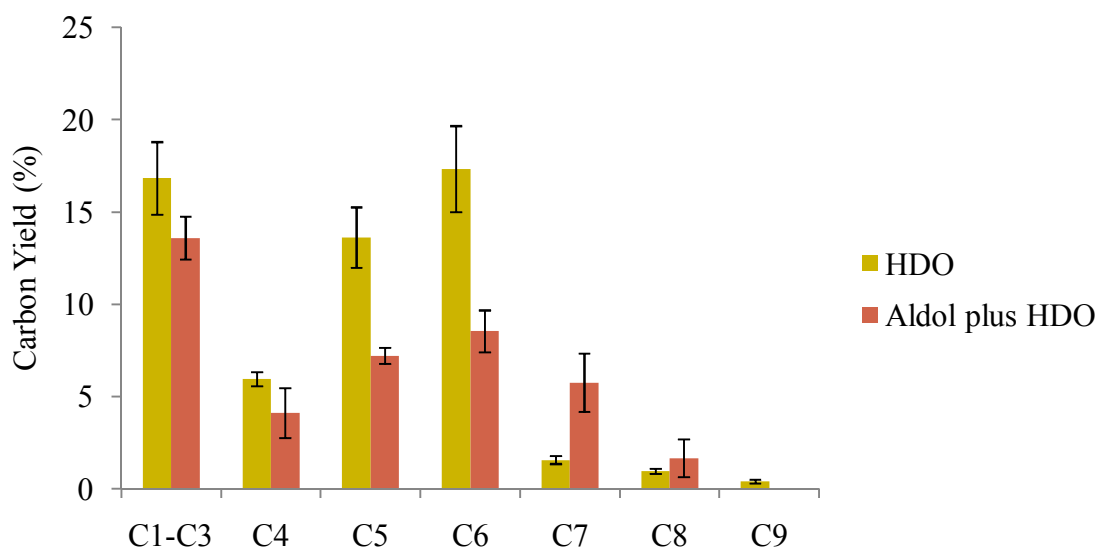


Figure 4: Product carbon distribution from the aldol condensation and sequential hydrodeoxygenation of cellulose over Cu/TiO₂ and PtMo/MWCNTs at 300°C and 3 bar H₂

As can be seen from Figure 4, the addition of the aldol condensation catalyst results in significantly reduced carbon yields to C₅ and C₆ products with increases to C₇ and C₈ hydrocarbons. Although self-aldol condensation of glycolaldehyde monomers resulted in the formation of C₃-C₇ products, the relative rise in products in this range in the cellulose system is inconsistent with C₂ and C₃ aldehydes serving as the major aldol condensation reactants. Unlike with glycolaldehyde, the rise in C₇ and C₈ yields is not accompanied by an increase in intermediate C₄ yields. Instead of glycolaldehyde self-coupling to form C₇₊ products, C₁-C₄ aldehydes and ketones may instead undergo cross-coupling with C₅ and C₆ molecules. Furfural-based molecules including 5-hydroxymethylfurfural, 5-methylfurfural, and furfural itself are present in pyrolysis feed streams. Furfural cannot undergo self-aldol condensation due to its lack of the hydrogen atom at the α -C required to form an enolate, and hydrogenation of the carbonyl group is favored over hydrogenation of the furan ring, so a hydrogen at the α -C will not be generated in situ [46–48]. However, furfural can still undergo aldol condensation if another carbonyl-containing species forms an enolate, making it susceptible to aldol condensation with lighter oxygenates in the system including glycolaldehyde. Levoglucosenone may also be a key aldol condensation participant in this system. Levoglucosenone is produced in small quantities during fast pyrolysis of cellulose and can be produced via dehydration of levoglucosan [49–51]. Although levoglucosenone, like furfural, is unable to form an enolate, it lacks the aromaticity of a furan ring and could be selectively hydrogenated to allow for the formation of an enolate, allowing levoglucosenone and its partially hydrogenated derivative to undergo aldol condensation with levoglucosenone, furfural-type molecules, or lighter oxygenates such as glycolaldehyde. It should be noted that the slight increase in C₇ and C₈ yields does not fully explain the larger losses in C₅ and C₆ yields. It is hypothesized that this missing carbon remains on the Cu/TiO₂ surface as coke, either from aldol condensation of C₅ and C₆ pyrolysis products to form C₁₀₊ products or from other reactions involving these pyrolysis products that also lead to coke formation. In particular, the drop in C₅ and C₆ yields suggests that the major C₅ and C₆ pyrolysis products (levoglucosan, levoglucosenone, and furfural-type structures) are responsible for this coke formation. Condensation between partially-hydrogenated levoglucosenone and other C₅ and C₆ carbonyl-containing species may result in the formation of species that do not desorb easily from the catalyst surface, or that are susceptible to side reactions that lead to coke formation.

As with glycolaldehyde, the aldol plus HDO experiment was repeated at elevated hydrogen partial pressure to attempt to limit coke formation due to sequential aldol condensation on the Cu/TiO₂ surface. The results of these experiments can be seen in Figure 5. As with glycolaldehyde, some higher molecular weight products can be observed in the C₉₊ range at the higher hydrogen pressure. However, this is accompanied by a sharp decrease in carbon yield to C₁-C₃ products. One possible explanation for this is that glycolaldehyde is consumed in significant amounts during aldol condensation, but additional C₁-C₃ molecules are generated via C-C bond cleavage reactions of aldol condensation products over PtMo/MWCNTs. Additional experiments are required to fully explain these results.

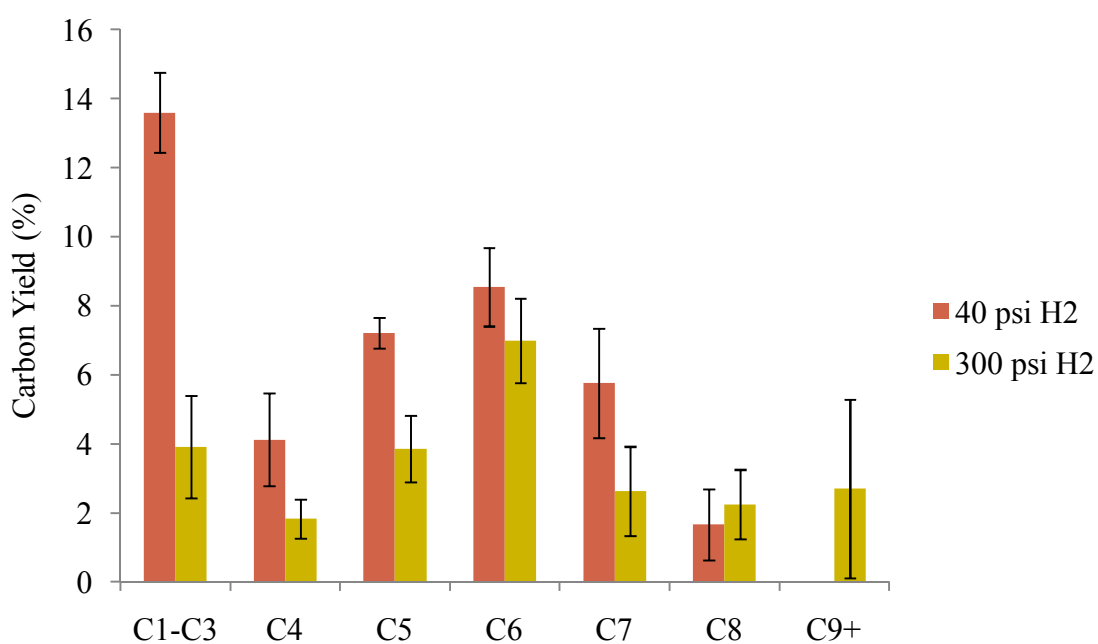


Figure 5: Product carbon distribution from the aldol condensation and sequential hydrodeoxygenation of cellulose over Cu/TiO₂ and PtMo/MWCNTs at 300°C and 40 psi H₂ or 300 psi H₂

3.2 Aldol Condensation of Butanal in the Continuous-Flow Fixed Bed Reactor

The Cu/TiO₂ catalyst was studied in the continuous flow fixed-bed reactor in order to determine the effect of the addition of a hydrogenation function to a known aldol condensation catalyst, TiO₂. Following preliminary studies conducted using the previously described pyroprobe unit, butanal was chosen as a model compound for further study in the continuous-

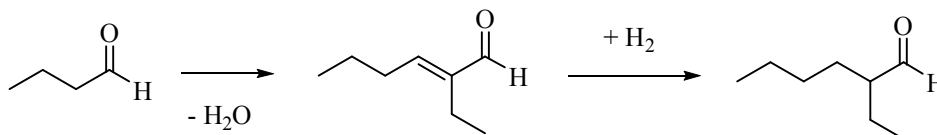
flow fixed bed reactor. Although commonly studied feeds for aldol condensation including butanal but also acetaldehyde and propanal are easy to obtain commercially, the applicability of these model compound studies to pyrolysis vapors from intact biomass is unclear. Although studies with butanal can give information about the behavior of the catalyst with a simple aldehyde, there is additional complexity in pyrolysis vapors that is not captured by a straight chain alkanal. Glycolaldehyde itself, the target molecule for these studies, has a hydroxyl group bound to the α -C. As described previously, aldol condensation proceeds through an enolate intermediate on the catalyst surface. The effect of a hydroxyl group on the α -C may be important, and is not represented in butanal. In addition, the complexity of pyrolysis vapors is not well-represented by butanal. TiO_2 is known to deactivate rapidly during aldol condensation due to multiple aldol condensation reactions taking place and forming coke on the surface of the catalyst [19,24]. Larger oxygenates than the C_2 glycolaldehyde may also bind to the surface and form coke; pyrolysis of lignin leads to the formation of phenolic products, and in addition to levoglucosan, these products may adsorb to the surface of the catalyst. If these molecules undergo aldol condensation, they may form much larger products which do not desorb from the surface of the catalyst. Nevertheless, examining a model compound such as butanal can give basic insight into the effect of the addition of a hydrogenation function to the catalyst on the reaction pathway. Therefore, studies were conducted in a continuous-flow fixed-bed reactor to determine the extent to which the addition of a hydrogenation promoter would impact the product carbon distribution.

3.2.1 Aldol Condensation of Butanal over Cu/TiO_2

Based on the pyroprobe results, more detailed studies on Cu/TiO_2 were performed using butanal as the model compound. Products are categorized into C_4 products, C_8 products, and $>\text{C}_8$ products. Butanol and butane account for 99% of carbon selectivity to C_4 products. Butene is also observed in trace amounts. Butanal is not included in C_4 products, as it is the reactant. Although butanoic acid is detected in the product stream from this reaction, it is present in the same abundance as it is in a product stream from a reactor without catalyst. Subtracting this blank therefore shows no statistically significant butanoic acid formation over the Cu/TiO_2 catalyst. Butanoic acid is likely present as an impurity in the reactant butanal stream. It is also possible to form butanoic acid through an esterification reaction, only to break the ester apart in

the presence of hydrogen into butanoic acid and butane. This is unlikely, however, as butanoic acid is present in much larger quantities than butane; if butanoic acid is included in the analysis, it accounts for approximately 6% of carbon selectivity, as compared to <1% carbon selectivity towards butane at steady state. Therefore, butanoic acid is not included as a C₄ product, but is rather considered an impurity in the reactant stream.

A number of C₈ products, resulting from a single aldol condensation, are observed in the product stream. The dominant C₈ product was 2-ethyl-hexenal, with a minor product 2-ethyl-hexanal, as shown in Reaction 4. Additionally, <1% carbon selectivity was observed towards hydrogenated alkanes and alkenes. These products were identified as isomers of octane and octene based on the maximum fragment seen in the MSD signal as well as on their elution times inside the GC capillary column. However there was insufficient signal for each in the MSD to identify specific isomers. 2-ethyl-hexane and 2-ethyl-hexene are likely two of these isomers, resulting from hydrogenation and hydrodeoxygenation of the major and minor products.



Reaction 4: Reaction pathway of butanal to form the two major C₈ products observed over 2% Cu/TiO₂

Additional C₈ products observed include 3-methyl-4-heptanone, butyl ester butanoic acid, and 2-ethyl-hexanoic acid, shown in Figure 6. Selectivity towards each of these products is in the range 0.5% - 1.5% at all conditions examined here. 3-methyl-4-heptanone could be formed through the hydrodeoxygenation of the aldehyde group following aldol condensation in place of the dehydration of the alcohol to form an alkenal. Butyl ester butanoic acid is likely formed through esterification of butanal. 2-ethyl-hexanoic acid is most likely formed from the reaction of the impurity butanoic acid with butanal.

>C₈ products includes all observed products from multiple aldol condensations. These products proved difficult to identify using the GC/MS techniques described here, due to the low concentrations of individual products and a lack of data for some of the expected aldol condensation structures in the NIST database used for EIMS analysis. Carbon numbers for these products are assumed based on peak elution times and maximum observed m/z. This approach

indicates that the $>C_8$ fraction consists primarily of C_{12} molecules, however at higher conversions there is significant carbon selectivity to C_{12+} products, with 7% of carbon going to these products at 63% conversion. Structures for C_{12} products were similarly unable to be identified due to low MSD signal and an incomplete library for the identification of C_{12} oxygenated products in the NIST software used to analyze MSD data. Aldol condensation and partial hydrogenation of C_8 products 2-ethyl-2-hexenal and 2-ethylhexanal are shown in Reaction 5 as the most likely candidates for the identity of these products.

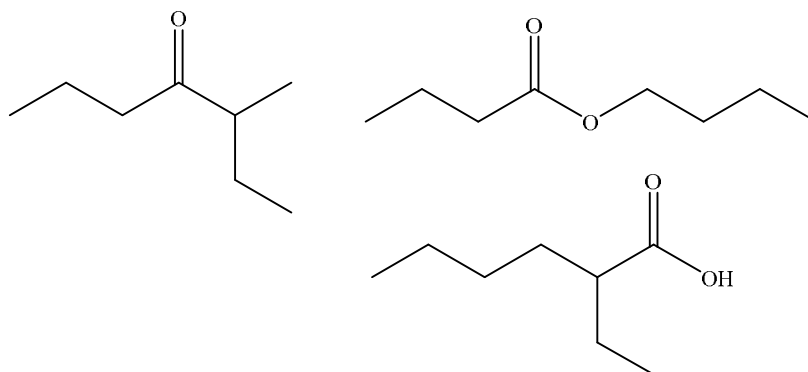
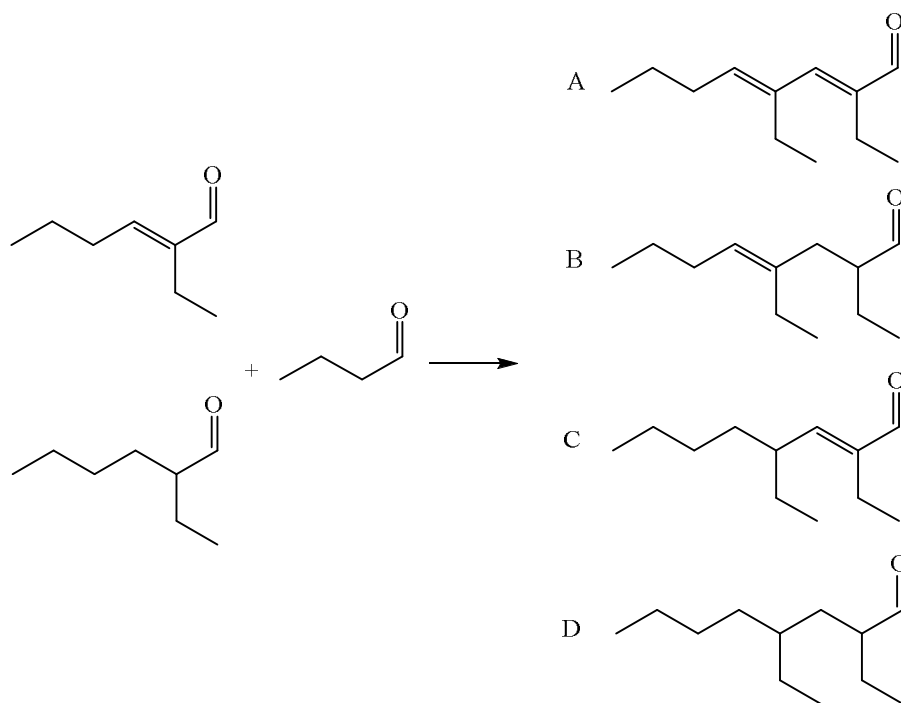


Figure 6: Structures for observed minor C_8 products. At the top from left to right: 4-methylheptanone and butyl ester butanoic acid. At the bottom: 2-ethyl-hexanoic acid

All of these structures are expected to be seen in the C_{12} portion of the product distribution, since aldol condensation products and their hydrogenated forms are observed in the C_8 fraction. A dominant C_{12} product is observed, but none of these structures have reported EIMS fragmentation patterns. This C_{12} product dominates the C_{12} portion of the product distribution, with approximately 9% total carbon selectivity towards this single product at the highest conversion examined. Some hints as to the correct structure of this product are provided by the elution time of the major C_{12} product in the GC. In all of the Cu/TiO₂ experiments, no significant products are observed after the major C_{12} product. The capillary column used separates products by boiling point such that 2-ethyl-hexenal elutes after 2-ethyl-hexanal; the major product is therefore most likely Product A, (2,4)-diethyl-(2,4)-octadienal.



Reaction 5: Aldol condensation products from the reaction between the major C₈ products with a second butanal molecule to form C₁₂ products. A, B, C, and D are structures which could be observed as C₁₂ products assuming no further reactions take place.

Structure A, (2,4)-diethyl-(2,4)-octadienal, is formed through aldol condensation between the primary condensation product, 2-ethyl-2-hexenal, and butanal without subsequent hydrogenation of the C-C double bonds. Although product A would likely be the dominant product of a second aldol condensation reaction, it is also possible that the observed major C₁₂ product undergoes a second reaction such as that seen in the aldol condensation of acetone in which a ring product is formed [25], as shown previously in Reaction 1. Finally, the largest m/z with significant abundance in the EIMS spectra for the major C₁₂ product is 180, one possible molecular formula for which is C₁₂H₂₀O, the molecular formula of structure A. In order to confirm this peak assignment, each of these structures would need to be synthesized and injected into the GCMS as standards. By varying the space velocity with several different loadings of catalyst, product carbon selectivity has been mapped as a function of conversion over the range of 5% butanal conversion to 70% butanal conversion. Figure 7 shows the results from these experiments. As seen here, selectivity towards C₈ products increases over 5% to 15% conversion with corresponding decrease in selectivity towards C₄ products. As conversion increases, Selectivity

towards $>C_8$ products begins to increase with corresponding decrease in selectivity towards C_8 products.

From Figure 8, it is seen that 2-ethyl-hexenal is the dominant product, with 85% selectivity at 15% conversion and 50% selectivity at 63% conversion. At very low conversions, butanol selectivity decreases with increasing 2-ethyl-hexenal, reflecting the increase in selectivity towards aldol condensation over hydrogenation.

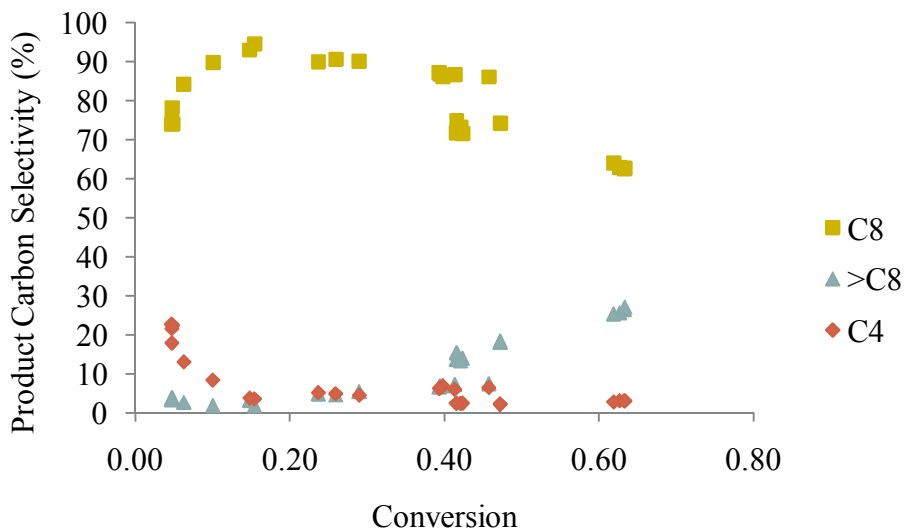


Figure 7: Selectivity to products by number of aldol condensations as a function of conversion over 2% Cu/TiO₂ at 300°C and 1 bar H₂

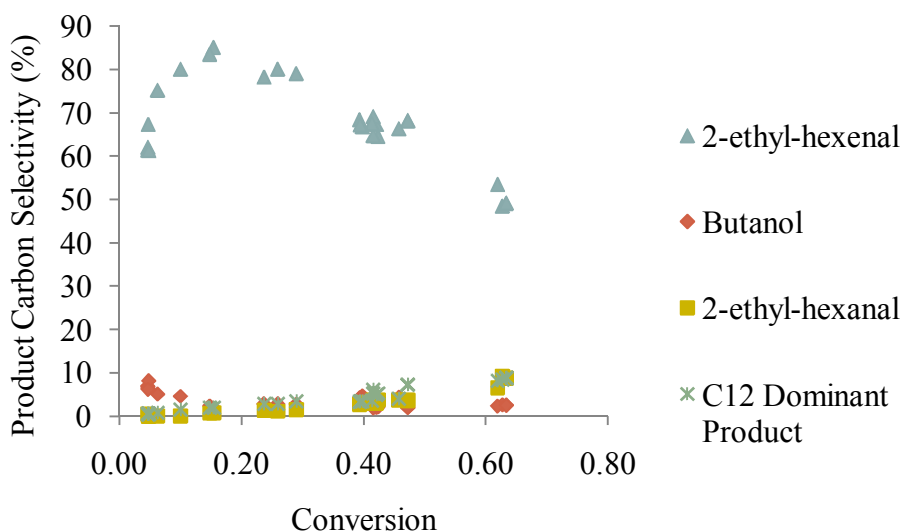


Figure 8: Carbon selectivity to the major observed products as a function of conversion over the 2% Cu/TiO₂ catalyst at 300°C and 1 bar H₂

As selectivity towards 2-ethyl-hexenal increases, the reaction is driven towards secondary reactions to form 2-ethyl-hexanal and the C₁₂ major product, the selectivities towards each of which increase over time. This is shown in greater detail in Figure 9. Here, a monotonic increase in selectivity towards 2-ethyl-hexanal and the C₁₂ major product is seen.

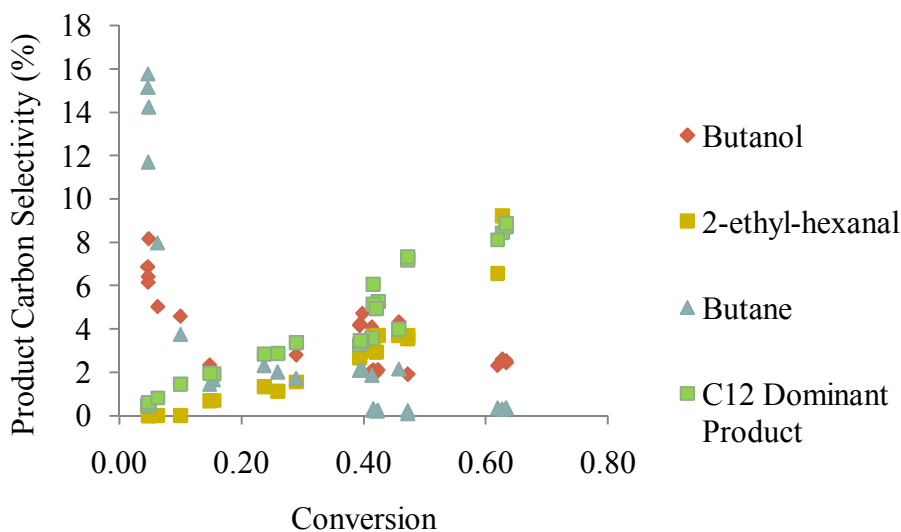


Figure 9: Expanded view of carbon selectivity to the minor products (carbon selectivity < 10%) as a function of conversion over 2% Cu/TiO₂ at 300°C and 1 bar H₂

As seen in Figure 9, selectivity towards 2-ethyl-hexenal and the major C₁₂ product increases with increasing conversion, with corresponding decrease in selectivity towards 2-ethyl-hexenal. 2-ethyl-hexenal and the major C₁₂ product are secondary reaction products, with 2-ethyl-hexenal as the direct precursor to each product. At low conversions, it can be seen that selectivity towards C₄ products and 2-ethyl-hexenal is relatively high. Here, selectivity towards the major C₁₂ product is low, while there are additional C₁₂ products that may be observed with much lower selectivity and which elute earlier in GCMS than the major C₁₂ product. These products could be the result of aldol condensation between 2-ethyl-hexenal and butanal or of esterification of 2-ethyl-hexenal with butanal.

3.2.2 2% Cu/TiO₂ Deactivation during Aldol Condensation of Butanal

Deactivation is an important issue with aldol condensation over TiO₂ catalysts. Here, catalyst deactivation may be studied in the continuous-flow reactor. As seen in Figure 10, on start-up the catalyst experiences rapid deactivation with later activation with a final steady-state

conversion reached after approximately 5 hours on stream. When selectivity is plotted as a function of time for these same experiments in Figure 11, initial catalyst deactivation appears to follow a pattern in which increasing 2-ethyl-hexenal selectivity is accompanied by decreasing secondary product selectivity and decreasing conversion. 2-ethyl-hexenal is produced by hydrogenation of the double bond in 2-ethyl-hexenal, while $>C_8$ products are produced by aldol condensation of 2-ethyl-hexenal with a second butanal molecule. This would indicate that the changes in conversion as a function of time are caused by a change in reactivity of 2-ethyl-hexenal bound to the surface of the catalyst.

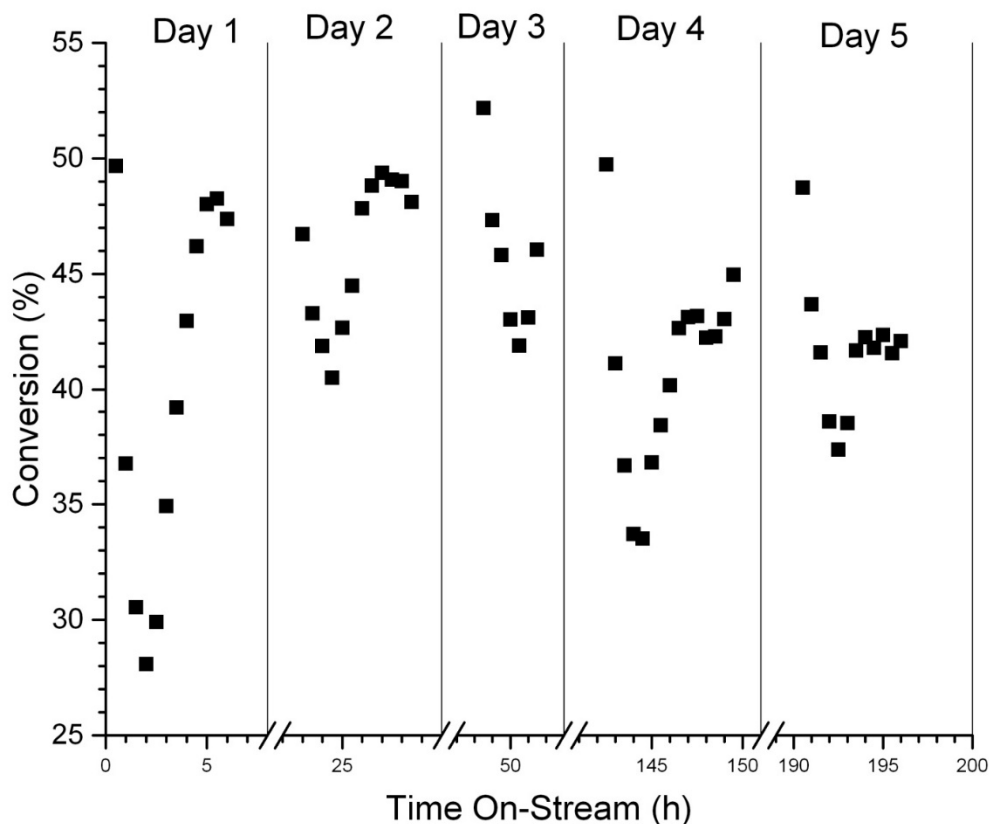


Figure 10: Deactivation of 2% Cu/TiO₂ at moderate conversion

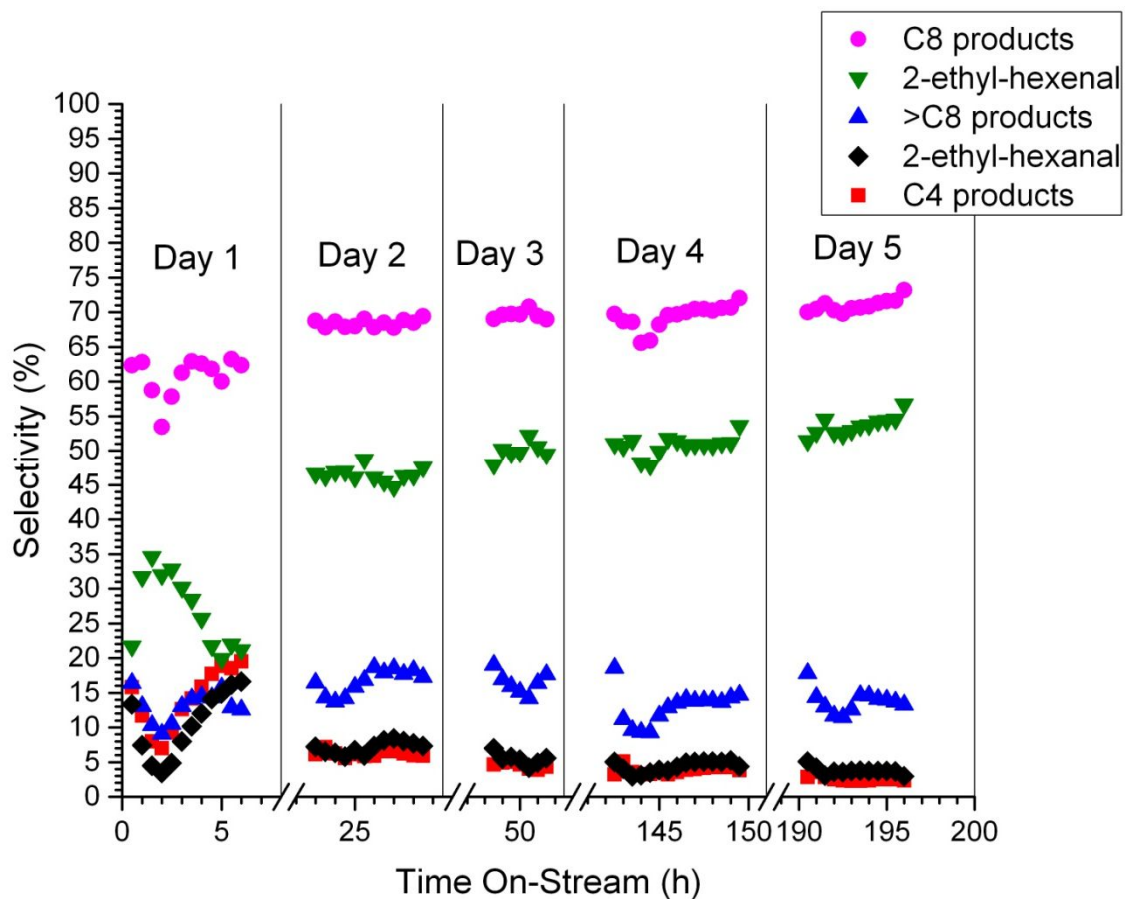


Figure 11: Deactivation behavior of 2% Cu/TiO₂ at moderate conversion: dynamic product carbon distribution

At low conversions, where selectivity towards C₁₂ products is decreased in favor of C₄ products, it could be expected that selectivity towards the multiple aldol condensations which are hypothesized to be responsible for coke formation would be decreased, leading to decreased catalyst deactivation. This is shown in Figure 12 with a lower loading of 2% Cu/TiO₂. From this plot, it is seen that although initial deactivation remains severe, the catalyst appears to be more stable in the long term than at higher conversions.

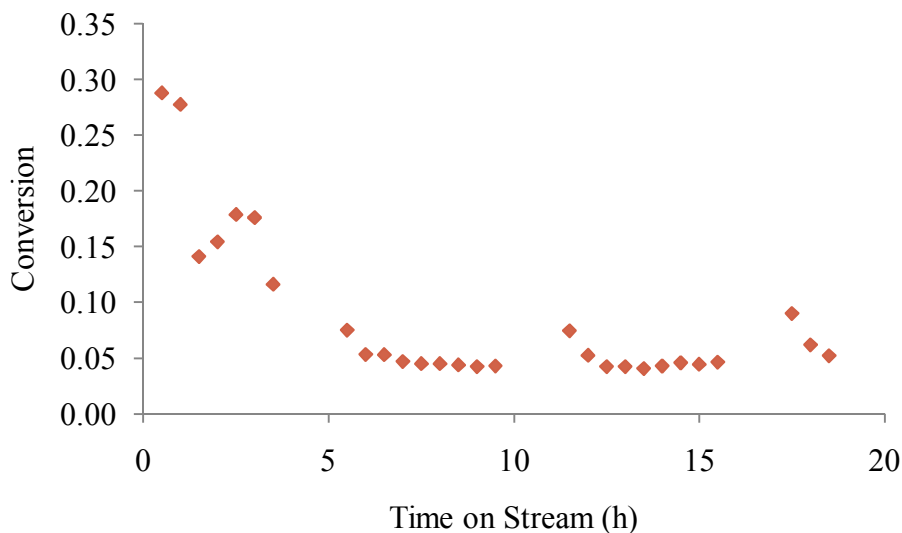


Figure 12: Stability of Cu/TiO₂ at low conversion

From Figure 10 and Figure 11, it is not obvious that the system is at steady-state when conversion begins to plateau after approximately 5 hours of run-time; it is important for the system to be at steady-state during the space velocity runs presented previously. Insufficient data was collected during a full day of running the reactor to clearly describe the behavior of the catalyst. To resolve this, additional data was collected over an extended period of time. The conversion vs. time data and selectivity vs. time data from these experiments are shown in Figure 13 and Figure 14, respectively. From these plots, it can be seen that after the catalyst has undergone initial deactivation, catalyst re-activation gives rise to a steady-state conversion which only slowly decreases, indicating that the catalyst has roughly stabilized and that the previous data were collected at steady-state conditions.

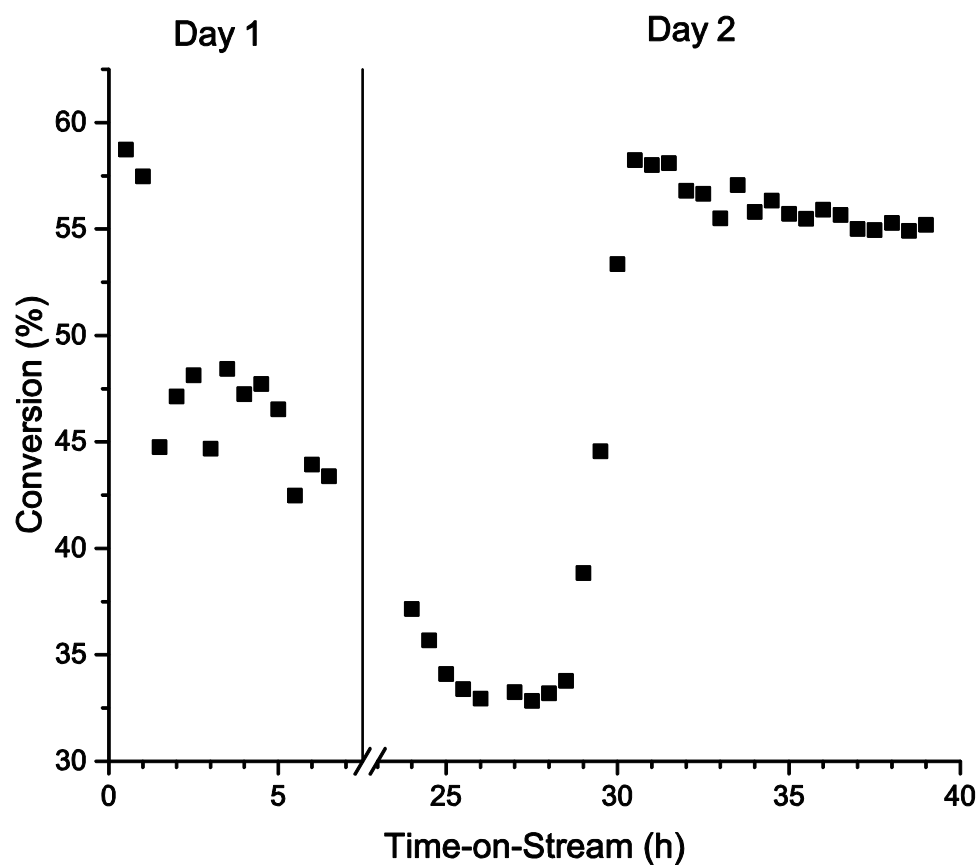


Figure 13: Stability of 2% Cu/TiO₂ over 16 hours

However, in this data it can be seen that conversion and selectivity on the first day of running the reactor do not follow the same trends as they did in previous experiments. Specifically, initial deactivation on the first day of running is much more severe, and product selectivities do not exhibit extrema in the data from the extended runs as they do in the original data.

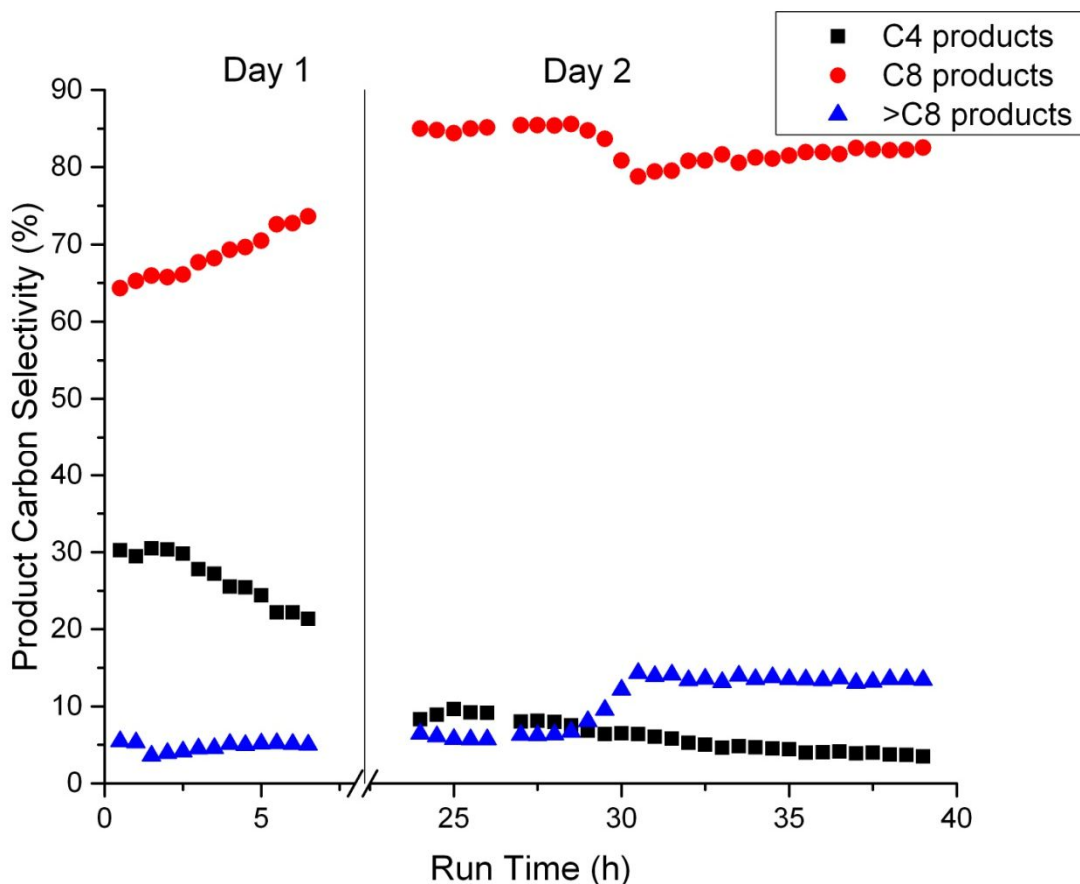


Figure 14: Stability of 2% Cu/TiO₂ over 16 hours: dynamic product distribution

Experiments were also conducted to examine the regeneration of the Cu/TiO₂ catalyst. At the end of a day of runs, the standard procedure for these experiments is to allow the catalyst to sit in low flows of hydrogen and helium overnight, until the next time that the reaction is performed. In these experiments, the overnight flow of hydrogen was turned off, so that only helium passed over the catalyst overnight. The conversion vs. time results can be seen in Figure 7. In the wake of temporarily shutting off hydrogen flow, conversion uniformly decreased by approximately 10%. However, the daily trend in conversion was unaffected, indicating that two forms of regeneration are likely taking place. Given that the extended runs saw no oscillations in conversion as a function of time, it is likely that a minimum in the conversion is reached only once after butanal flow is turned on; afterwards, the catalyst reaches a state where slow deactivation takes place over time. It is this slow deactivation that is likely regenerated by hydrogen. A minimum in conversion data only reappears after butanal flow is turned on after a

night of being turned off, indicating that the sites responsible for initial deactivation are being regenerated in overnight hydrogen flow.

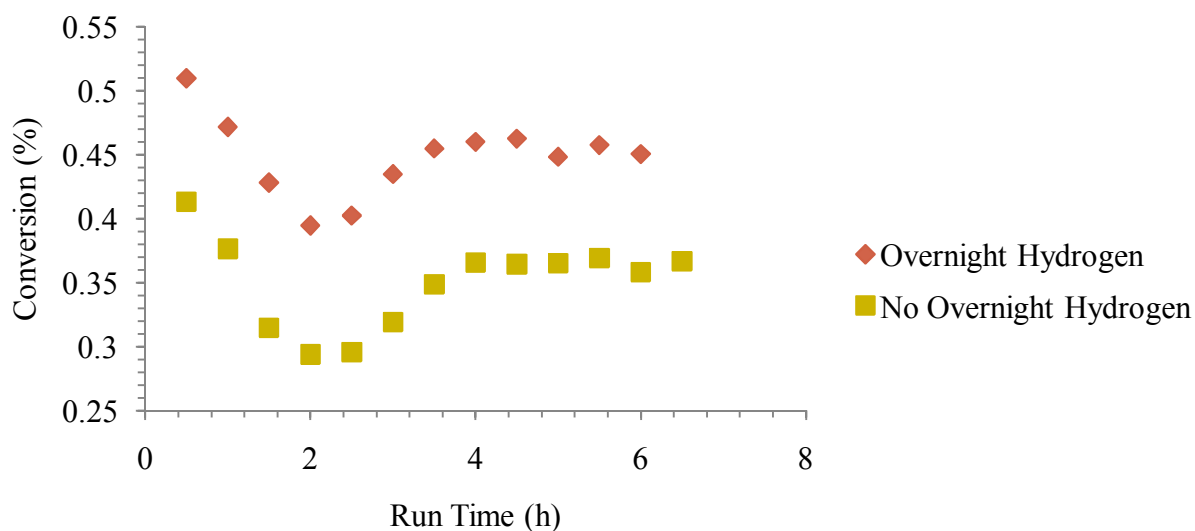


Figure 15: Effects of overnight hydrogen flow on 2% Cu/TiO₂

3.2.3 Aldol Condensation of Butanal over TiO₂

In order to investigate the impact of copper in the Cu/TiO₂ catalyst, TiO₂ was studied in the model compounds unit. Cu was hypothesized to contribute the hydrodeoxygenation and hydrogenation activity observed in the Cu/TiO₂ results. Therefore, it was expected that with TiO₂ alone there would be decreased selectivity towards C₄ products as well as the minor C₈ product, 2-ethyl-hexanal. As can be seen in Figure 16, the TiO₂ catalyst alone shows very low selectivity towards C₄ products of approximately 2%, with similar selectivity towards butane and butanol.

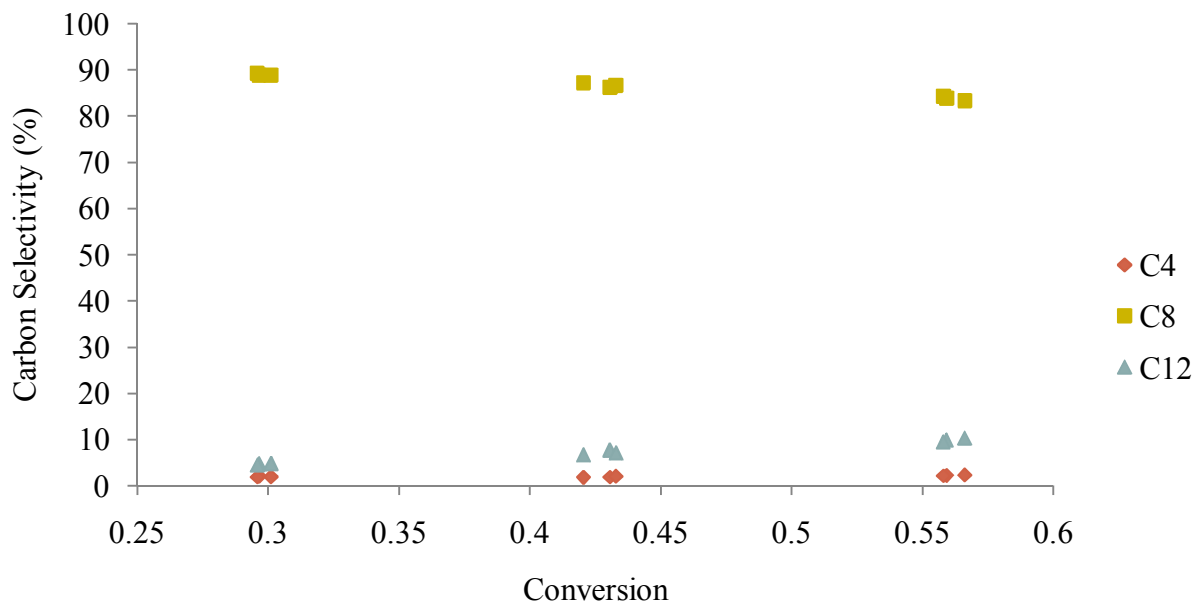


Figure 16: Product carbon distribution from aldol condensation of butanal over TiO₂ at 300°C and 1 bar H₂

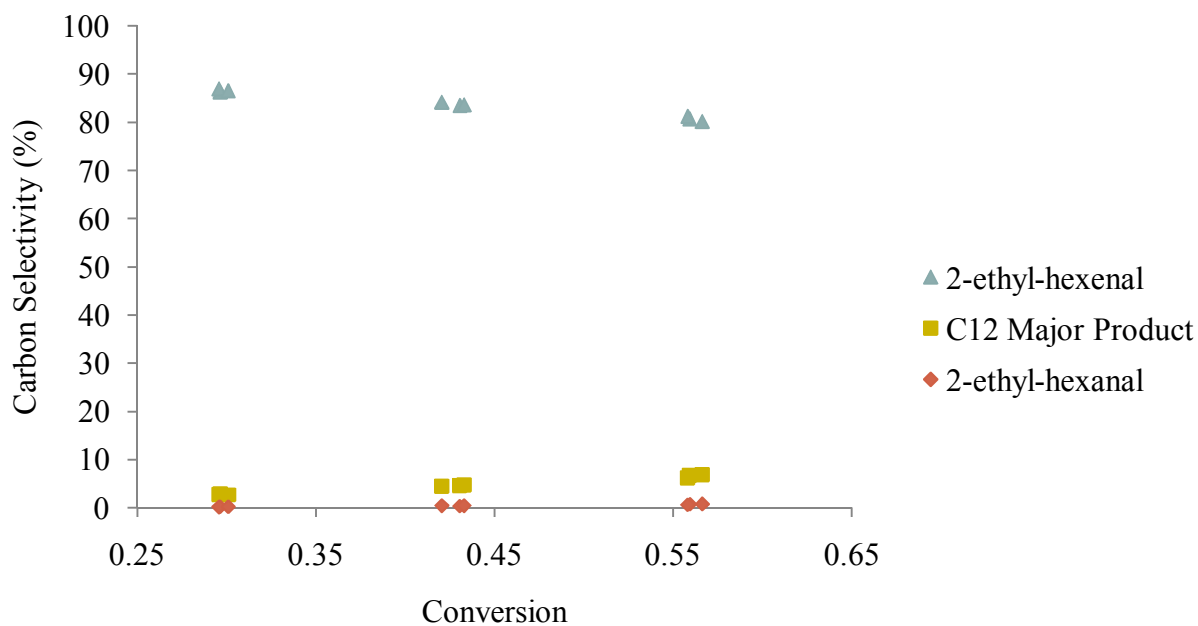


Figure 17: Product carbon distribution for major products over TiO₂ at 300°C and 1 bar H₂

The major products over the Cu/TiO₂ catalyst were 2-ethyl-hexenal, 2-ethyl-hexanal, and an unidentified C₁₂ product. The selectivity towards these specific products over TiO₂ over the

conversion range of 30% to 60% is shown in Figure 17. As seen here, there is negligible selectivity towards 2-ethyl-hexanal over the TiO_2 catalyst. This is consistent with previous work, which has shown that TiO_2 alone does not hydrogenate $\text{C}=\text{C}$ or $\text{C}=\text{O}$ bonds at low H_2 pressures [19,20,24,40]. Once again, the major C_{12} product could not be identified, but had the same retention time as the major C_{12} product seen from 2% Cu/TiO_2 . Previously, it was argued that the major C_{12} product from aldol condensation over Cu/TiO_2 was a product from the aldol condensation of the major C_8 product, 2-ethyl-hexenal, and not 2-ethyl-hexanal. This argument is supported by the TiO_2 data. The major C_{12} product from the TiO_2 experiments has an identical retention time inside the Supelco SPB-1 capillary column as the major C_{12} product from the Cu/TiO_2 experiments. In addition, the MS spectra gathered from the major C_{12} product from TiO_2 and 2% Cu/TiO_2 are shown in Figure 18 and Figure 19, respectively. The fragmentation patterns are identical. This is a strong indication that they are the same product, even though clear identification was not possible. Since TiO_2 alone does not exhibit significant hydrogenation activity to form 2-ethyl-hexanal, this product is likely formed through reaction of the 2-ethyl-hexenal product. Additionally, this is evidence that the major observed C_{12} product is not an ester product, as work by Wang, Goulas, and Iglesia has shown that TiO_2 is not active for esterification at similar conditions to the work done here [24].

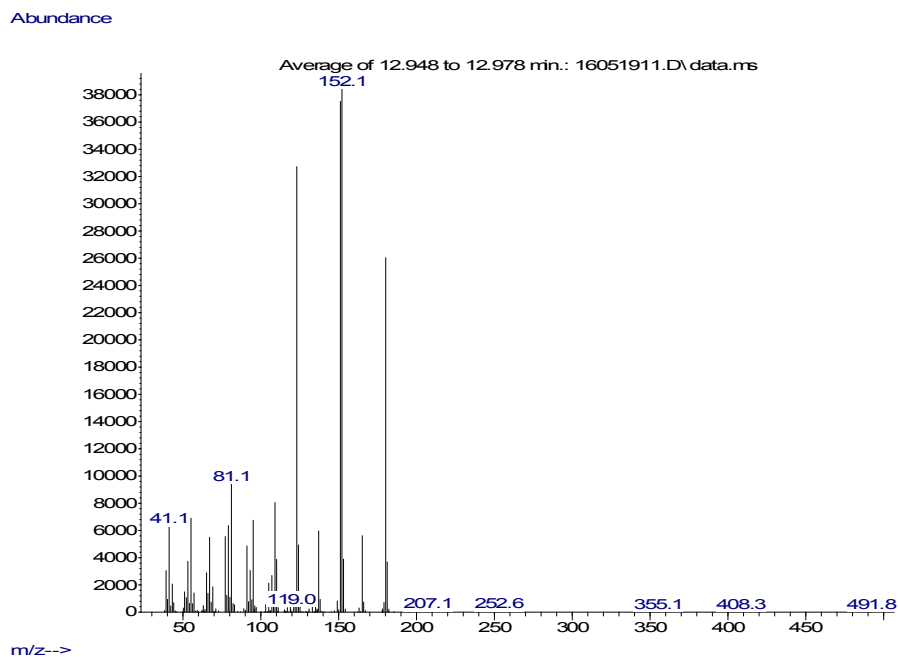


Figure 18: MS EI fragmentation pattern for the major C₁₂ product from aldol condensation of butanal over TiO₂

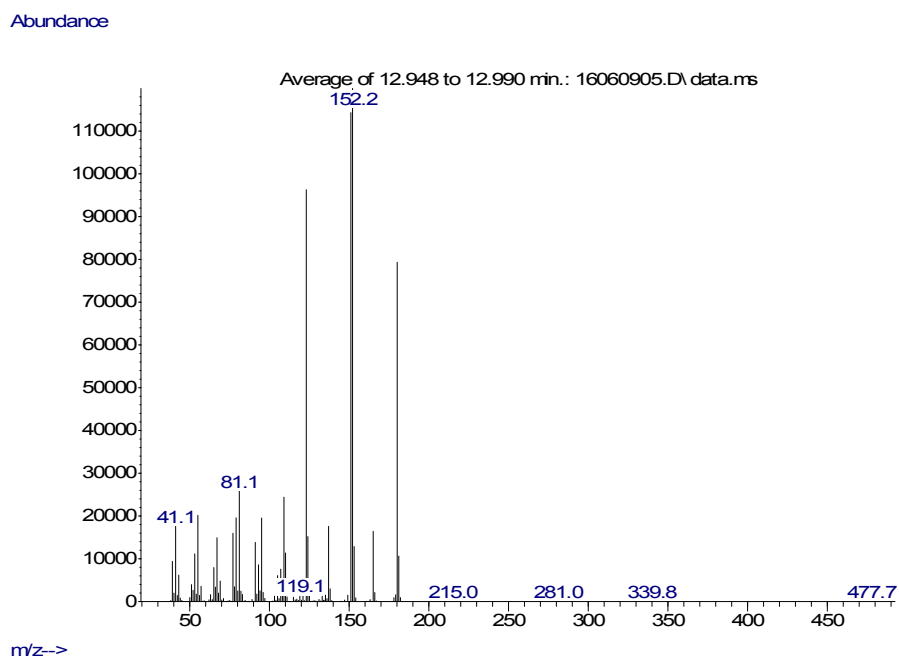


Figure 19: MS EI fragmentation pattern for the major C₁₂ product from aldol condensation of butanal over 2% Cu/TiO₂

3.2.4 TiO₂ Stability during Aldol Condensation of Butanal

As with the 2% Cu/TiO₂ catalyst, TiO₂ stability was briefly examined on the continuous flow reactor. Conversion as a function of time on stream for one loading of catalyst is shown in Figure 20.

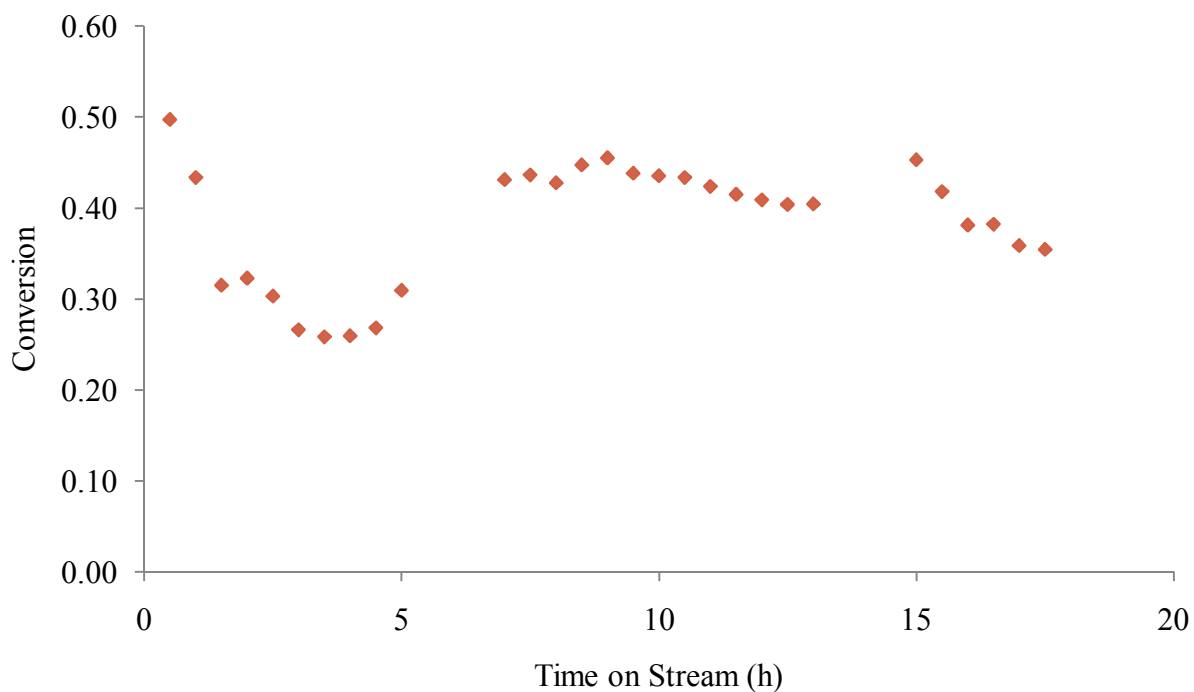


Figure 20: Stability of TiO₂ at moderate to low conversion

TiO₂ exhibits initial deactivation and catalyst reactivation in the first set of runs, but this is not repeated followed by prolonged exposure to hydrogen in the absence of butanal between runs. This implies that Cu may be involved in catalyst regeneration, possibly through the slow hydrogenation and hydrodeoxygenation of strongly adsorbed aldol condensation products. Further work is necessary in order to clarify the differences in catalyst deactivation between TiO₂ and Cu/TiO₂, such as through an investigation of a series of Cu/TiO₂ catalysts with varying Cu loadings.

Figure 21 shows the carbon selectivity towards the major C₈ product, 2-ethyl-hexenal, as a function of time on stream over TiO₂. Figure 22 shows the carbon selectivity towards all C₄ and C₁₂ products as a function of time on stream. From these plots, it can be seen that with fresh catalyst, a sharp decrease in selectivity towards the double condensation C₁₂ products from 16%

to 6% is accompanied by a sharp increase in selectivity towards 2-ethyl-hexenal from 75% to 83% in the first two hours of running the reactor. Initially, some sites are blocked, resulting in fewer sets of three or more adjacent catalytic sites (which would allow for the adsorption and reaction of butanal molecules for the formation of C₁₂ products). This explains the accompanying increase in 2-ethyl-hexenal selectivity.

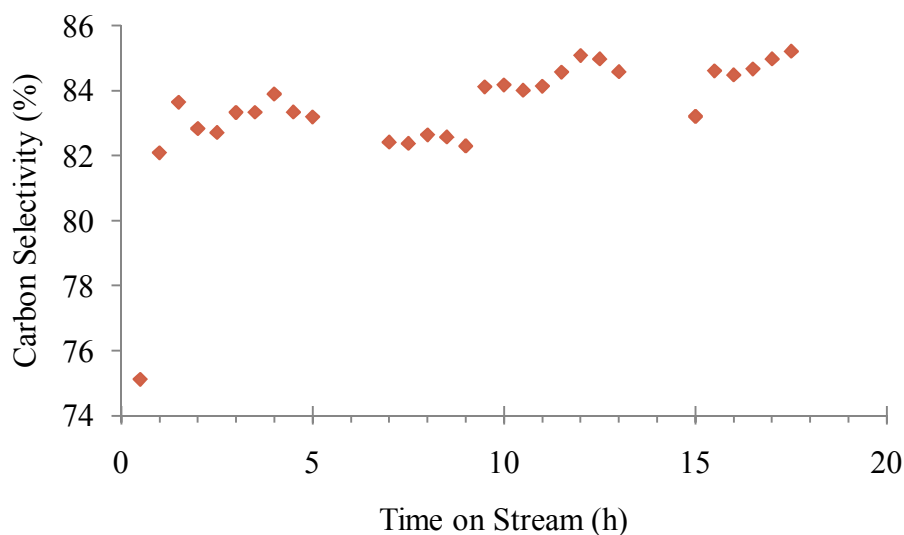


Figure 21: Stability of TiO₂ at moderate to low conversions: carbon selectivity to the major product, 2-ethyl-hexenal

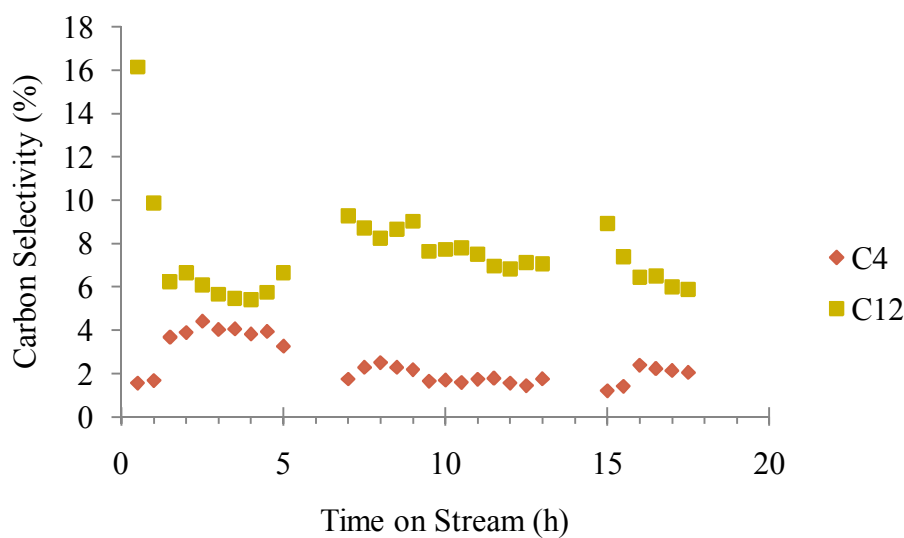


Figure 22: Stability of TiO₂ at moderate to low conversions: carbon selectivity to minor products

3.3 Effects of feedstock on product carbon distribution

The effects of different feedstocks on the product carbon distribution may be studied using a cyclone reactor which has previously been reported [2,6]. However, preliminary experiments may be conducted using the pyroprobe reactor. These materials were subjected to pyrolysis and HDO over the 5% PtMo/MWCNT catalyst in the pyroprobe unit. 20.4 bar H₂ was used to ensure complete HDO of pyrolysis products. HDO was conducted at 300°C, with pyrolysis at 500°C.

3.3.1 Pyrolysis plus HDO of Genetic Variants

Another pathway to value-added products lies in the genetic modification of biomass source materials. Lignin is composed of p-hydroxyphenyl (H), guaiacyl (G), and syringyl (S) subunits, shown in Figure 23, coupled together by a variety of linkages, the most common of which is the β -O-4 linkage [52].

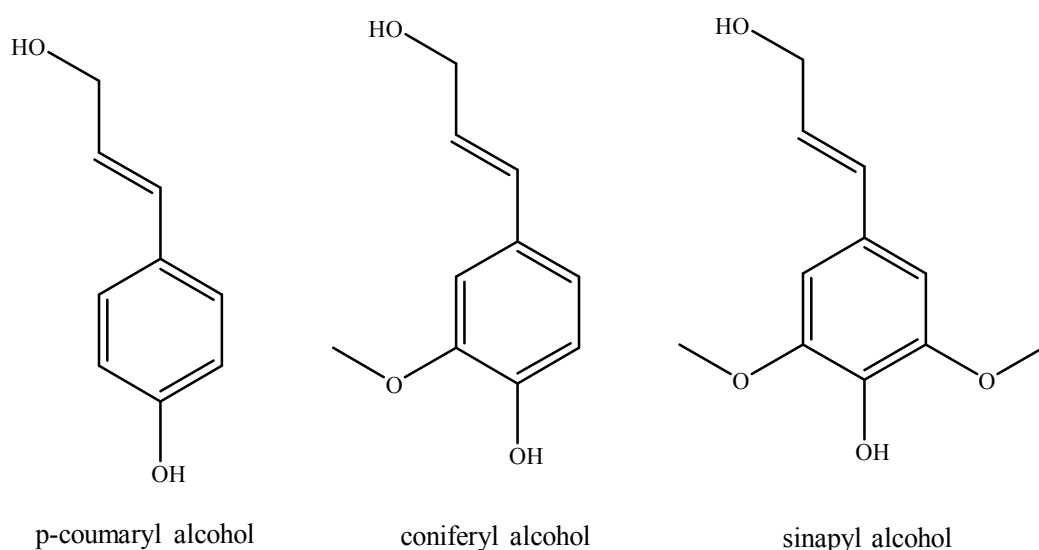


Figure 23: Monomers of lignin. p-coumaryl alcohol forms H units, coniferyl alcohol forms G units, and sinapyl alcohol forms S units.

One proposed method of increasing overall selectivity to value-added products is to genetically modify a feedstock plant such that it exhibits varying relative proportions of the lignin monomers. Poplar has been genetically modified to vary the ratio of the S unit to the G unit [53,54]. These materials have previously been studied by the Abu-Omar group in their studies of the removal of lignin from intact biomass and its selective conversion to 2-methoxy-4-propylphenol and 2,6-

dimethoxy-4-propylphenol, which has shown that high-S poplar gives high selectivity towards 2,6-dimethoxy-4-propylphenol, while high-G poplar gives high selectivity towards 2-methoxy-4-propylphenol but at lower overall yield to desired products [14]. It has been proposed that the relative abundances of the lignin subunits could also have an effect on the product distribution of the H₂Bioil process, either on the molecules produced or on the carbon efficiency of pyrolysis. Wild type poplar, high-S poplar, and high-G poplar were subjected to fast hydrolysis and subsequent hydrodeoxygenation over 5% PtMo/MWCNTs in the pyroprobe reactor. As can be seen from Figure 24, there is no difference in product carbon selectivity between the wild type poplar samples and the high-G and high-S samples. Hydrodeoxygenation of intact biomass yields multiple isomers for product carbon numbers of 4 and greater, the details of which are shown in Appendix A. There is no significant variation in any specific product across the three poplar genotypes examined.

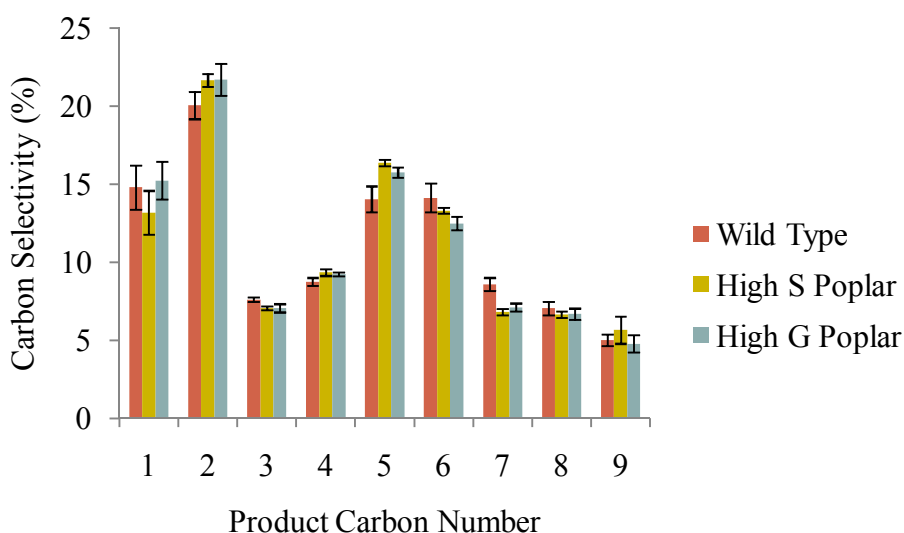


Figure 24: Carbon distribution by carbon number for HDO of poplar and poplar genetic variants over 5% PtMo/MWCNTs at 300°C and 20.4 bar H₂

Based on the structures of the S and G units, these results are as expected. Complete HDO would lead to the removal of methoxy groups and their transformation into methane. A slight change in selectivity towards methane would be expected, but from this result that change is within the error of the measurement. Furthermore, genetic modification had no effect on char production in these samples, with $30.4 \pm 1.8\%$ char yield for wild type poplar and $27.8 \pm 10.5\%$ and $29.8 \pm 9.4\%$ char yields for the high-G and high-S samples, respectively.

3.3.2 Pyrolysis plus HDO of CDL Residue

In addition to genetic modification, pre-treatment of biomass samples prior to pyrolysis for the purpose of transforming specific portions of biomass into more valuable chemicals may increase total selectivity of the process as a whole to desired products. Abu-Omar and coworkers have developed a Zn/Pd/C catalyst in methanol which performs catalytic depolymerization of lignin (CDL) through the cleavage of β -O-4 linkages [14,55,56]. This process results in the formation of the phenolic products 2-methoxy-4-propylphenol and 2,6-dimethoxy-4-propylphenol, but leaves behind a solid residue which is 12% lignin, 79% sugars, and 17% carbohydrates by mass; this is referred to as the carbohydrate residue [14]. Approximately 30% of carbon goes to char during fast-hydropyrolysis of poplar [2]. Lignin has been shown to be a major contributor to char formation in the fast pyrolysis of biomass [12]. A sample of the carbohydrate residue from the CDL process applied to poplar was therefore subjected to fast pyrolysis plus HDO over the PtMo/MWCNT catalyst in order to examine any changes to the carbon product distribution and to char formation compared to wild type poplar. These results were also compared to cellulose pyrolysis plus HDO. Figure 25 shows the results from these experiments.

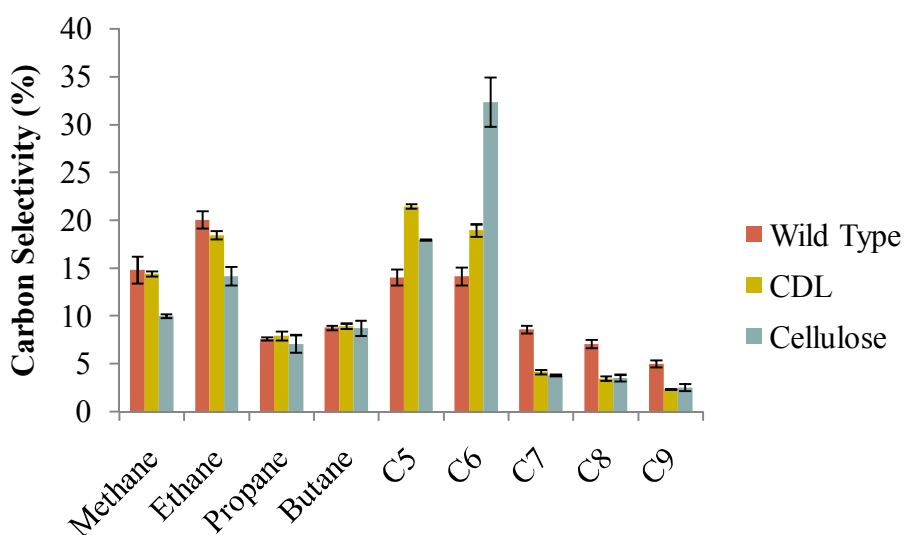


Figure 25: Product distribution by carbon number for HDO of wild type poplar, CDL residue from poplar, and cellulose over 5% PtMo/MWCNTs at 300°C and 20.4 bar H₂

A direct comparison of the C₆ products formed from the pyrolysis plus HDO of the wild type poplar and the CDL residue is shown in Figure 26, and a comparison of the C₇ products formed is shown in Figure 27. The product labeled “unidentified C₇” could not be identified using the NIST database, but was identified as a C₇ hydrocarbon based on elution time and on the presence of m/z of 98 as the maximum observed peak in the MSD. From the C₇ plot, it can be seen that the overall increase in selectivity to C₇ products observed in intact biomass relative to the residue from the CDL process is due to a much higher selectivity towards methylcyclohexane for the wild type sample. Methylcyclohexane is produced through HDO and hydrogenation of oxygenated toluene-based products, which are primarily lignin-derived. Similarly, differences in C₆ product carbon selectivity between the two samples can be traced back to differences in the relative abundances of cyclohexane, which is primarily derived from aromatic products produced from the pyrolysis of lignin, and hexane, which is formed primarily from the pyrolysis of cellulose and hemicellulose. A full breakdown of the product distribution by carbon number is given in Appendix B. It can be seen from these plots that the differences in product carbon selectivity between the wild type poplar sample and the CDL residue sample can be traced back to differences in selectivity towards aromatic-derived compounds such as methylcyclohexane, ethylcyclohexane, and propylcyclohexane.

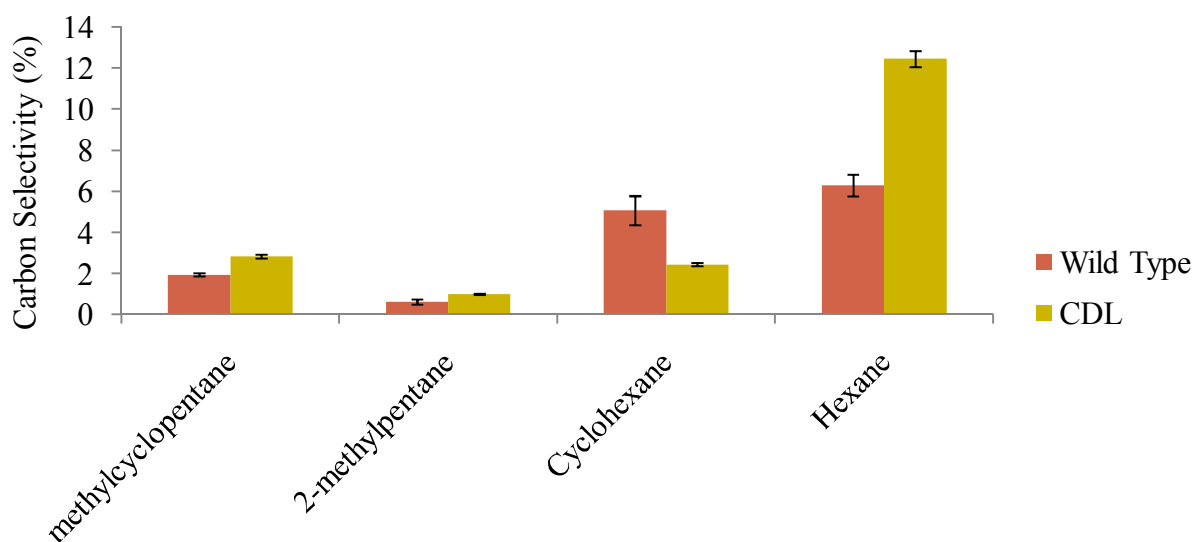


Figure 26: Carbon selectivity to specific C₆ products for HDO of poplar and CDL residue from poplar at 300°C and 20.4 bar H₂

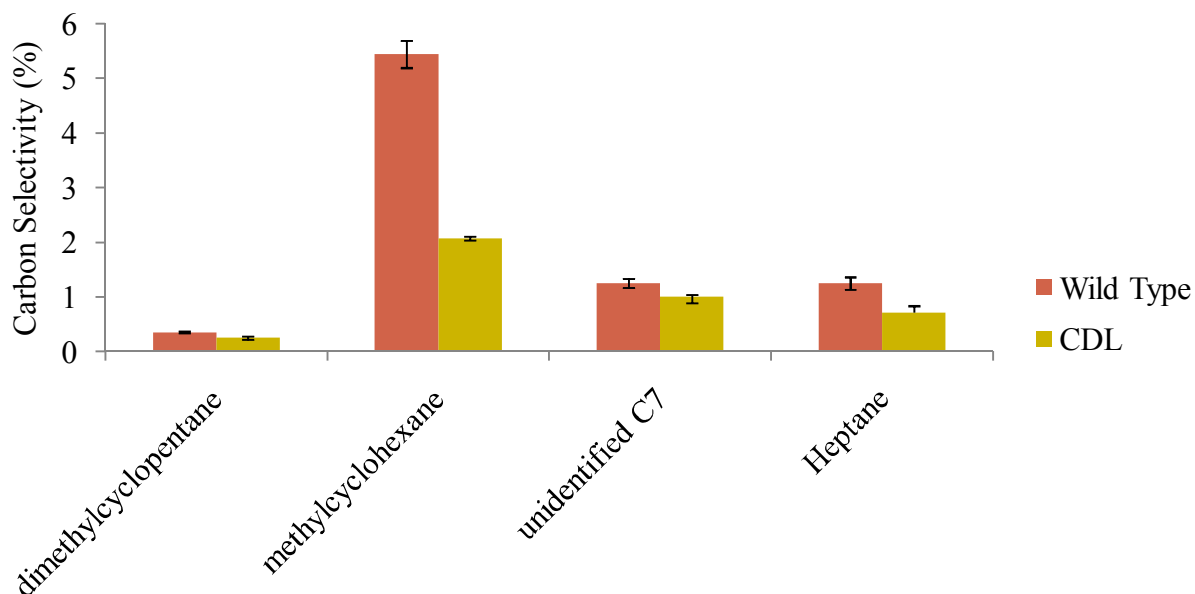


Figure 27: Carbon selectivity to specific C₇ products for HDO of poplar and CDL residue from poplar at 300°C and 20.4 bar H₂

Char formation was measured for the wild type and for the CDL residue samples, with the results shown in Table 2. There was no difference observed in char formation between the CDL samples and the wild type poplar samples. There are several possible explanations for this result. First, there is a small sample size of three measurements for each sample, but possibility for a large error in the char measurements for these samples. This is due to the high resolution needed to measure char masses. Biomass loadings on this unit are typically between 0.3 mg to 0.4 mg; following pyrolysis, between 0.04 and 0.1 mg of char are measured. The Mettler-Toledo XS205DU balance used for these measurements has a resolution of 0.01 mg. However, if small quantities of 0.01 mg of foreign material enter the quartz tube prior to char measurement, char masses will contain relatively large errors. In addition, a key assumption in these calculations is that char formed from the CDL residue has the same composition as char formed by cellulose, consisting of 81% carbon by mass as compared to 76% carbon by mass for wild-type poplar. The presence of inorganics, particularly alkali metals, have previously been shown to lead to char formation [57]. The CDL process is accomplished by a Pd/Zn/C catalyst. If small amounts of inorganics are left behind by this process, they could contribute to char formation. Finally, although cellulose shows extremely low char formation, it is possible that hemicellulose also

contributes to char formation [2]. Further work is needed to identify the source of char formed by pyrolysis of the CDL residue.

Feed	Char Carbon %
Wild Type	30 ± 2
CDL Residue	30 ± 2

Table 2: Carbon selectivity to char during pyrolysis of wild type poplar and CDL residue from poplar

4. CONCLUSIONS

2% Cu/TiO₂ has been shown to be active for aldol condensation of the model compound butanal. A dual-bed catalyst system with 2% Cu/TiO₂ followed by 5% PtMo/MWCNTs has been demonstrated to convert glycolaldehyde to higher hydrocarbons with significant competition from hydrodeoxygenation and hydrogenation pathways. However, this system has had limited success in application to cellulose pyrolysis vapors, where small increases in yields to C₇₊ hydrocarbons were accompanied by substantial carbon losses. There are several likely explanations for these results. First, extensive aldol condensation could be occurring on the surface of the 2% Cu/TiO₂ catalyst resulting in the formation of large products which are not desorbing from the surface of the catalyst. This would explain why low mass balance is observed for glycolaldehyde. Low mass balance would not be as easily detectable with cellulose because there are many more pyrolysis products from cellulose than glycolaldehyde which may be blocking catalytic sites and preventing the adsorption of oxygenates capable of performing aldol condensation. Thermogravimetric analysis should be done on catalysts from the aldol condensation of cellulose and of glycolaldehyde in order to quantify the carbon lost to coke during reaction to close the carbon balance for pyroprobe experiments. The high selectivity towards HDO products observed from glycolaldehyde may also be due to the formation of C-O bonds instead of C-C bonds through an esterification reaction over the Cu/TiO₂ catalyst. The PtMo catalyst would cleave these C-O bonds, resulting in high selectivity towards C₂ products from a glycolaldehyde feed. Recent work has suggested that the addition of a hydrogenation function to aldol condensation catalysts reduces coke formation through the formation of more stable saturated condensation products [24]. Aldol condensation of glycolaldehyde could therefore be further investigated by either increasing the Cu loading on TiO₂ or by incorporating a stronger hydrogenation promoter into the catalyst such as Pd or Pt in order to investigate the effects of limiting coke formation.

Additional reactions must be considered for upgrading cellulose fast pyrolysis products prior to aldol condensation. Although glycolaldehyde has been the target molecule of interest, it makes up less than 10 wt% of the product carbon distribution [6,9]. While it is desirable to convert C₂ products to larger molecules, levoglucosan makes up a much larger portion of the product distribution, with 50 wt% of final products [6,9]. Although levoglucosan lacks carbonyl

groups for aldol condensation, it can undergo dehydration to form levoglucosenone, which was discussed previously as a possible feed molecule for aldol condensation. Most critically, the ability of C₅ and C₆ carbonyl-containing species to undergo aldol condensation over Cu/TiO₂ must be investigated. Levoglucosenone and furfural-type molecules such as 5-hydroxymethylfurfural should be used as model compounds to determine the extent to which the Cu function is able to hydrogenate the C-C double bonds present in these structures that prevent formation of an enolate intermediate. Experiments considering self-coupling of these molecules in addition to cross-coupling with glycolaldehyde over Cu/TiO₂ should also be performed to understand the origins of C₇ and C₈ products in the cellulose aldol condensation system, as well as to understand the capacity of larger aldol condensation products from these molecules to form char on the TiO₂ surface.

Moving forward, catalysts need to be designed that will reduce selectivity towards multiple aldol condensation products due to the propensity of these products to remain on the catalyst surface as coke deposits. This may be possible by increasing the selectivity of the catalyst to hydrogenation products, either by increasing the copper loading on TiO₂ or by incorporating a stronger hydrogenation metal into the catalyst, such as Pd. Pt is likely too strong of a hydrogenation function, as initial experiments for aldol condensation plus hydrodeoxygenation in which PtMo/MWCNTs and Cu/TiO₂ were inadvertently mixed resulted in product distributions nearly identical to those of pure PtMo/MWCNTs, indicating that carbonyl groups would likely be removed before they had a chance to participate in aldol condensation in the presence of Pt. In addition to hydrogenation of reactive aldol condensation products, the binding strength of pyrolysis products to metal oxide aldol condensation catalysts should be investigated. With the current Cu/TiO₂ catalyst, strong binding of large pyrolysis or aldol condensation products to the surface could result in carbon losses and low overall yields toward C₇₊ products. In order to examine the potential poisoning effects of a complex pyrolysis product distribution containing many large oxygenates on the catalyst, a model compound such as butanal could be co-fed with 5-methylfurfural or dihydroeugenol in the continuous flow reactor in the absence of hydrogen. Under these conditions, 5-methylfurfural would act as a model compound for furfural-type molecules and dihydroeugenol would act as a model compound for lignin-derived pyrolysis products, allowing for the study of poisoning of the TiO₂ surface by fast pyrolysis products and inhibition of aldol condensation.

Although the work with genetic variants has shown that changes in the S/G ratio have no effect on pyrolysis plus HDO product distribution, it is possible that other genetic modifications to plants would result in a more promising feedstock for this process. However, since HDO removes all oxygen functional groups from pyrolysis products, lignin genetic modifications will likely have very little effect on the pyrolysis plus HDO product distribution. The S and G units differ primarily by the number of methoxy groups that each contains; under HDO, these will just be transformed to methane. Genetic modifications would have to result in longer carbon chain lengths without interruption by oxygen in order to give significant differences in the final product carbon distribution. However, genetic modifications have been shown to have greater impact on the product distribution of processes such as CDL. Although the CDL residue does not decrease char formation during pyrolysis relative to intact biomass, the product distribution is similar to that of cellulose. Coupling the CDL and H₂Bioil processes leads to the formation of both aromatic products through CDL and hydrocarbons through the H₂Bioil process. Additional refinement of the CDL process to improve the removal of lignin may lead to a feedstock which reduces overall char formation from the H₂Bioil process.

APPENDIX A. DETAILED PRODUCT DISTRIBUTION FOR THE PYROLYSIS AND HDO OF POPLAR GENETIC VARIANTS

For all products labeled “unidentified C_x,” products could not be identified from the MS signal using the NIST software due to low abundance of the product. These products are classified as C_x based on the maximum observed m/z and on the elution time.

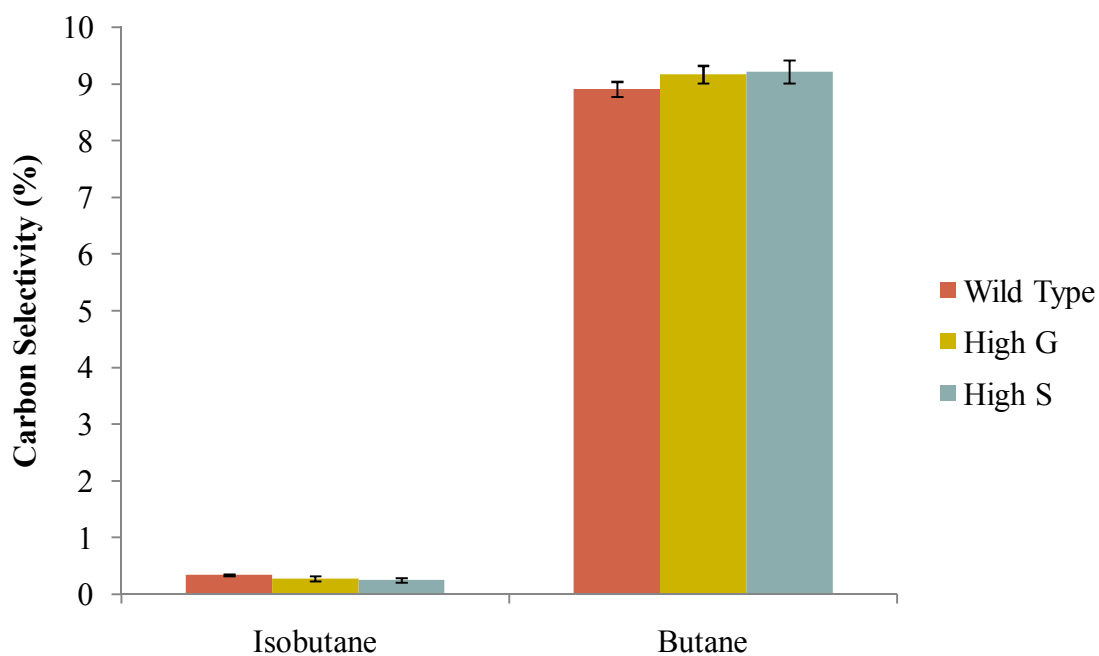


Figure 28: Carbon selectivity to specific C₄ products for HDO of poplar genetic variants at 300°C and 20.4 bar H₂

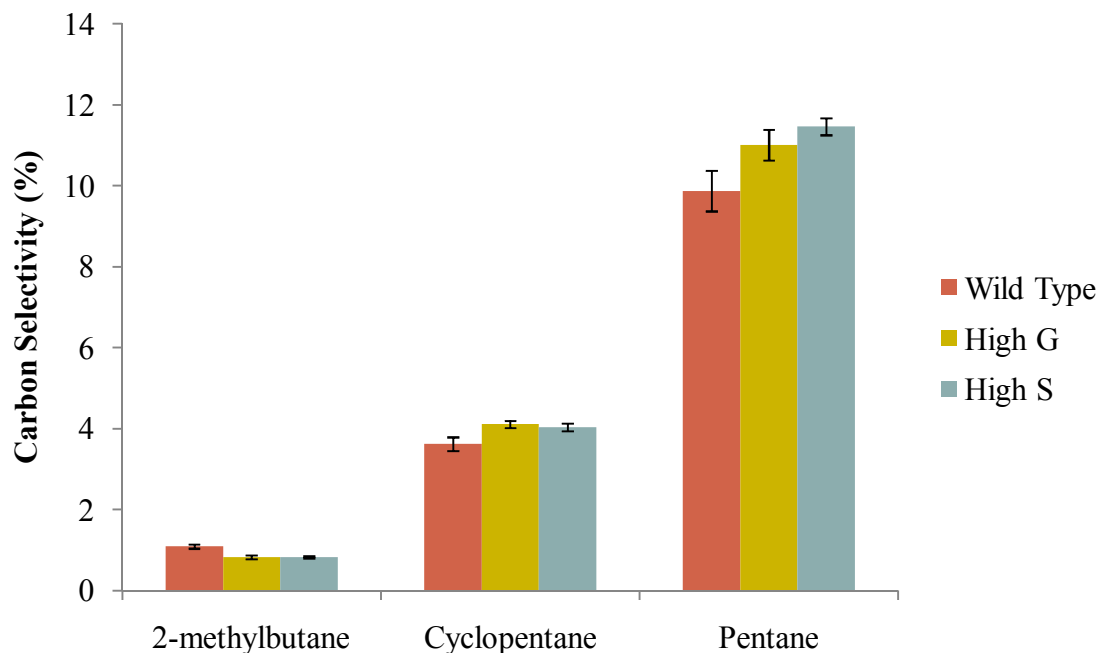


Figure 29: Carbon selectivity to specific C₅ products for HDO of poplar genetic variants at 300°C and 20.4 bar H₂

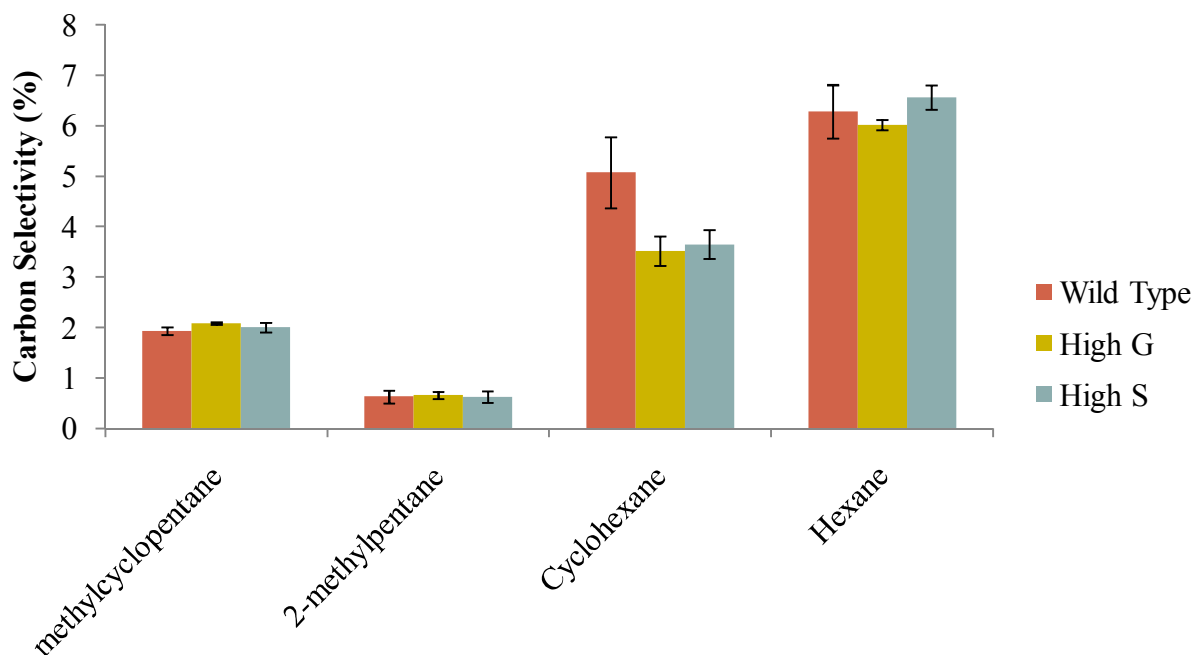


Figure 30: Carbon selectivity to specific C₆ products for HDO of poplar genetic variants at 300°C and 20.4 bar H₂

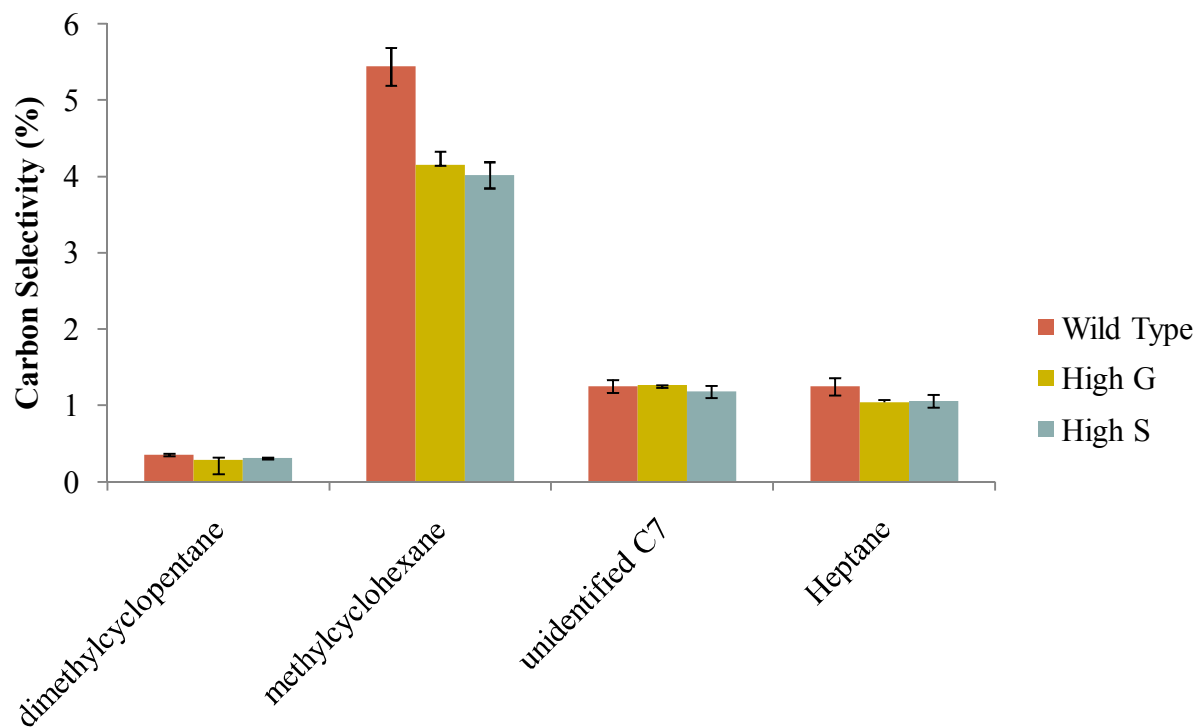


Figure 31: Carbon selectivity to specific C₇ products for HDO of poplar genetic variants at 300°C and 20.4 bar H₂

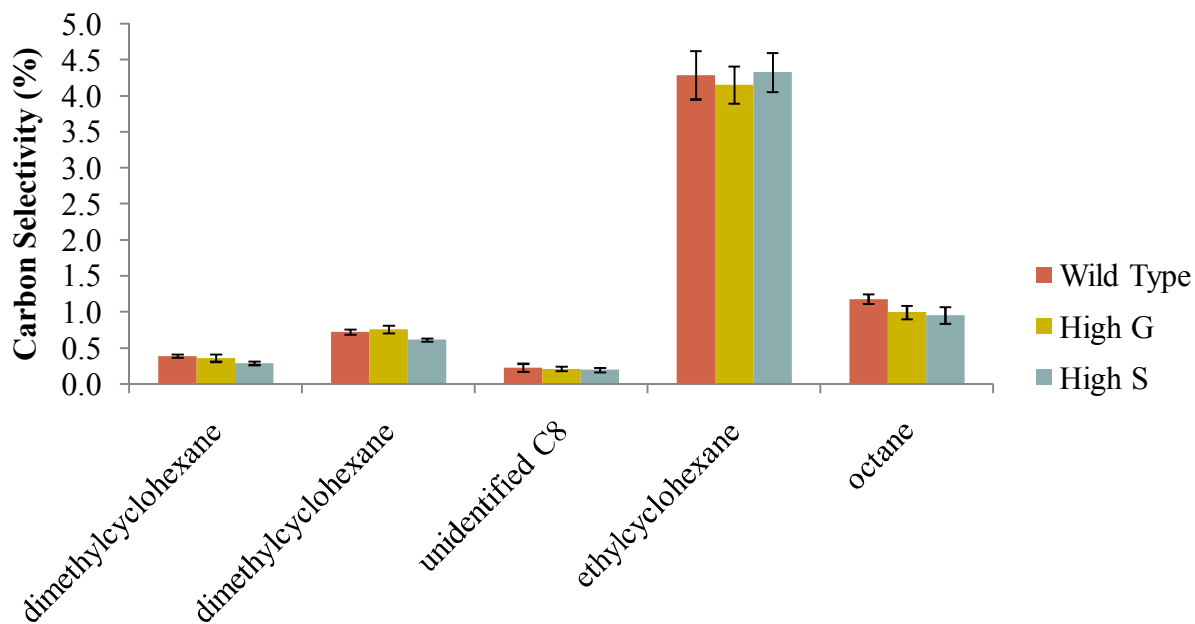


Figure 32: Carbon selectivity to specific C₈ products for HDO of poplar genetic variants at 300°C and 20.4 bar H₂

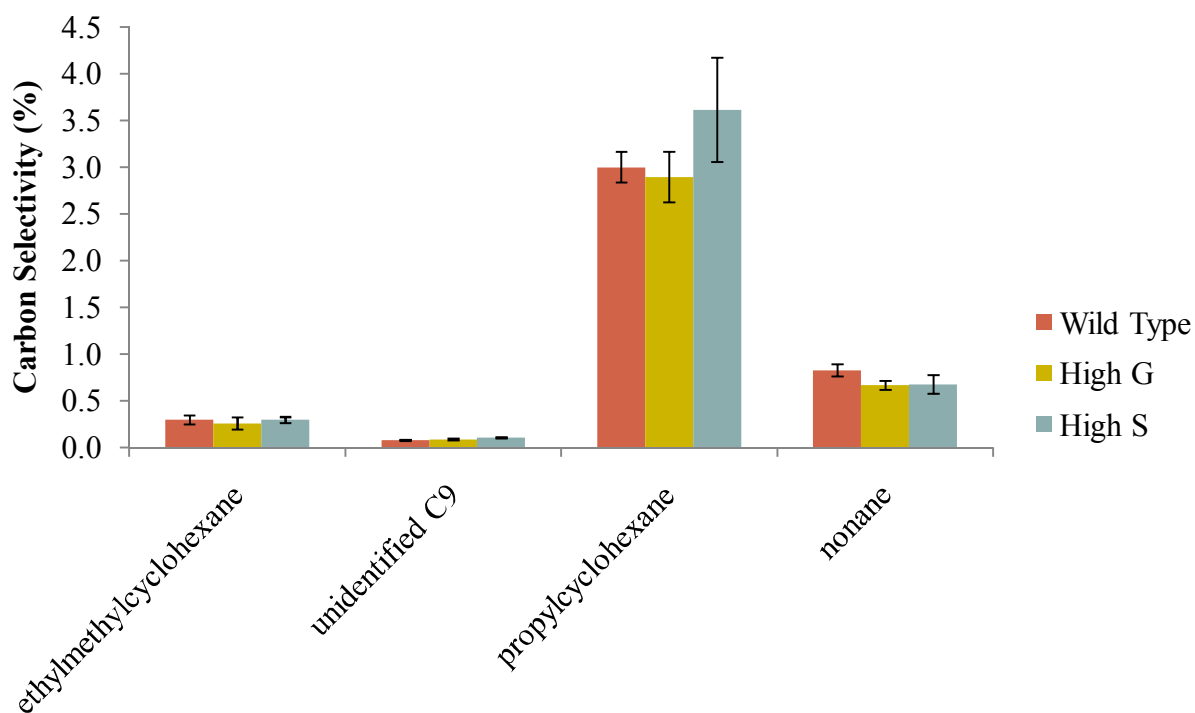


Figure 33: Carbon selectivity to specific C₉ products for HDO of poplar genetic variants at 300°C and 20.4 bar H₂

APPENDIX B. DETAILED PRODUCT DISTRIBUTION FOR THE PYROLYSIS AND HDO OF POPLAR CDL RESIDUE

For all products labeled “unidentified C_x,” products could not be identified from the MS signal using the NIST software due to low abundance of the product. These products are classified as C_x based on the maximum observed m/z and on the elution time.

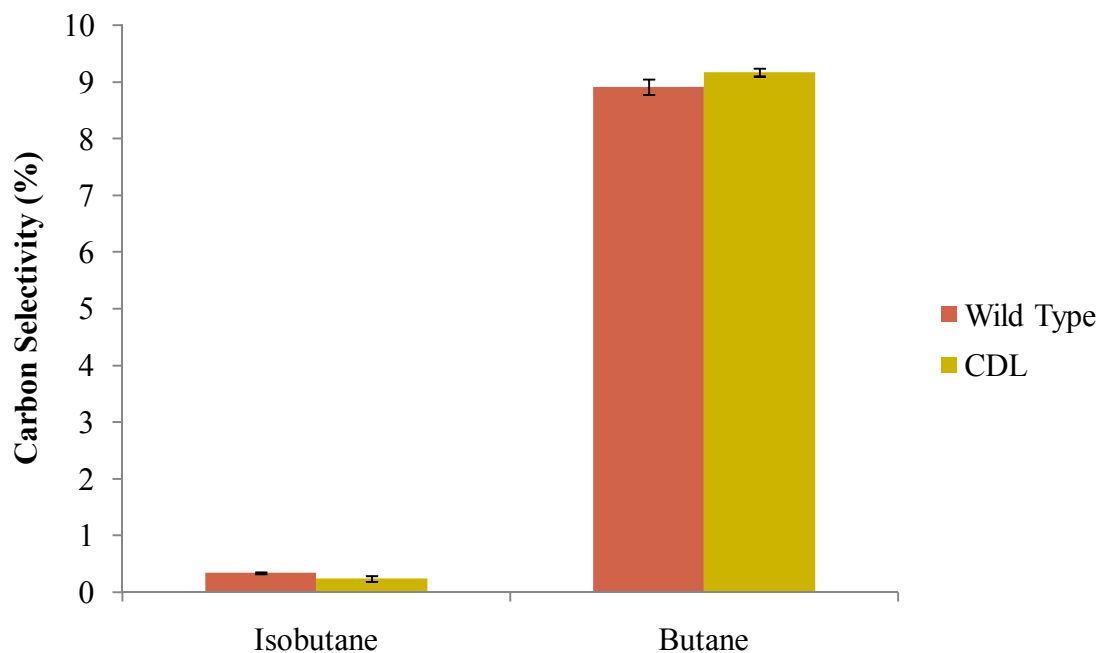


Figure 34: Carbon selectivity to specific C₄ products for HDO of poplar and CDL residue from poplar at 300°C and 20.4 bar H₂

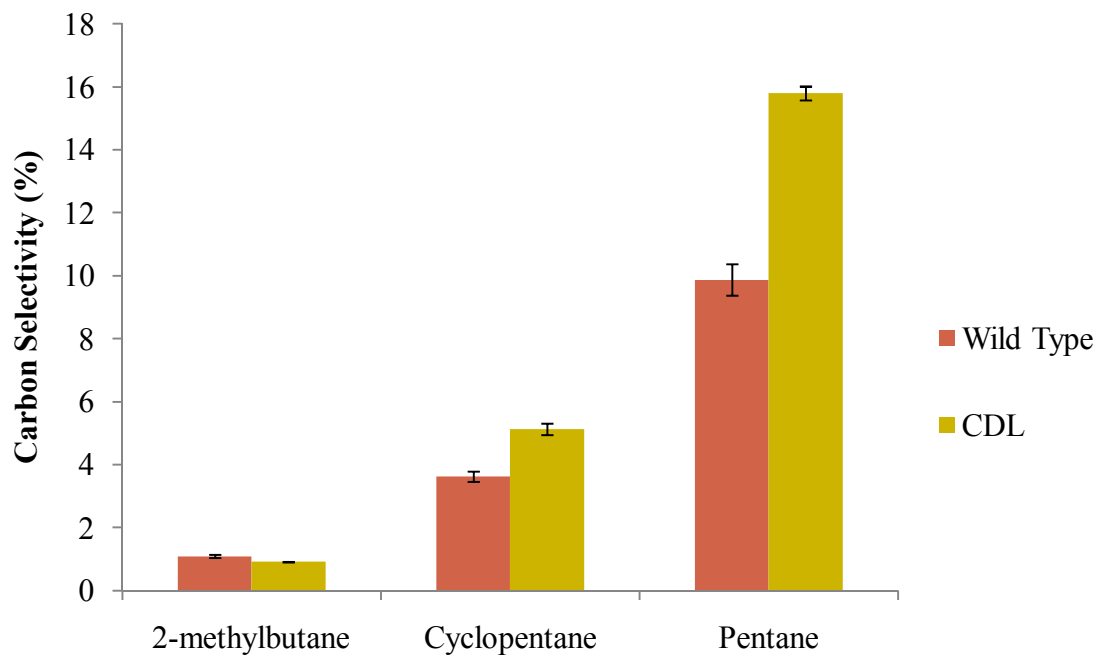


Figure 35: Carbon selectivity to specific C₅ products for HDO of poplar and CDL residue from poplar at 300°C and 20.4 bar H₂

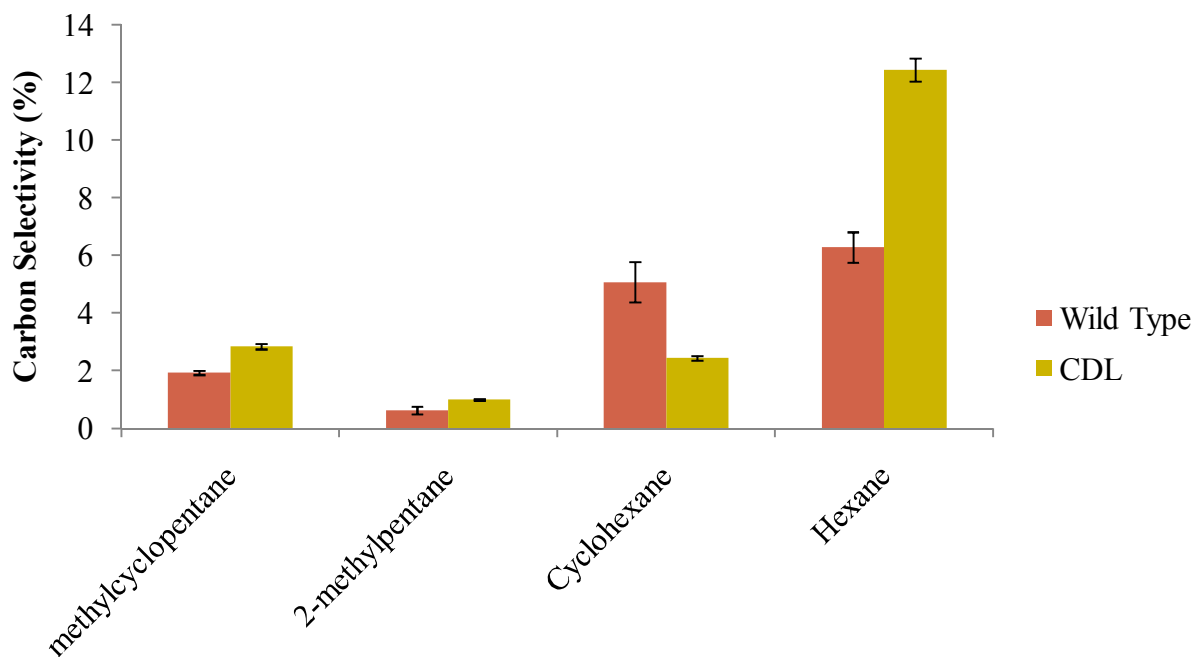


Figure 36: Carbon selectivity to specific C₆ products for HDO of poplar and CDL residue from poplar at 300°C and 20.4 bar H₂

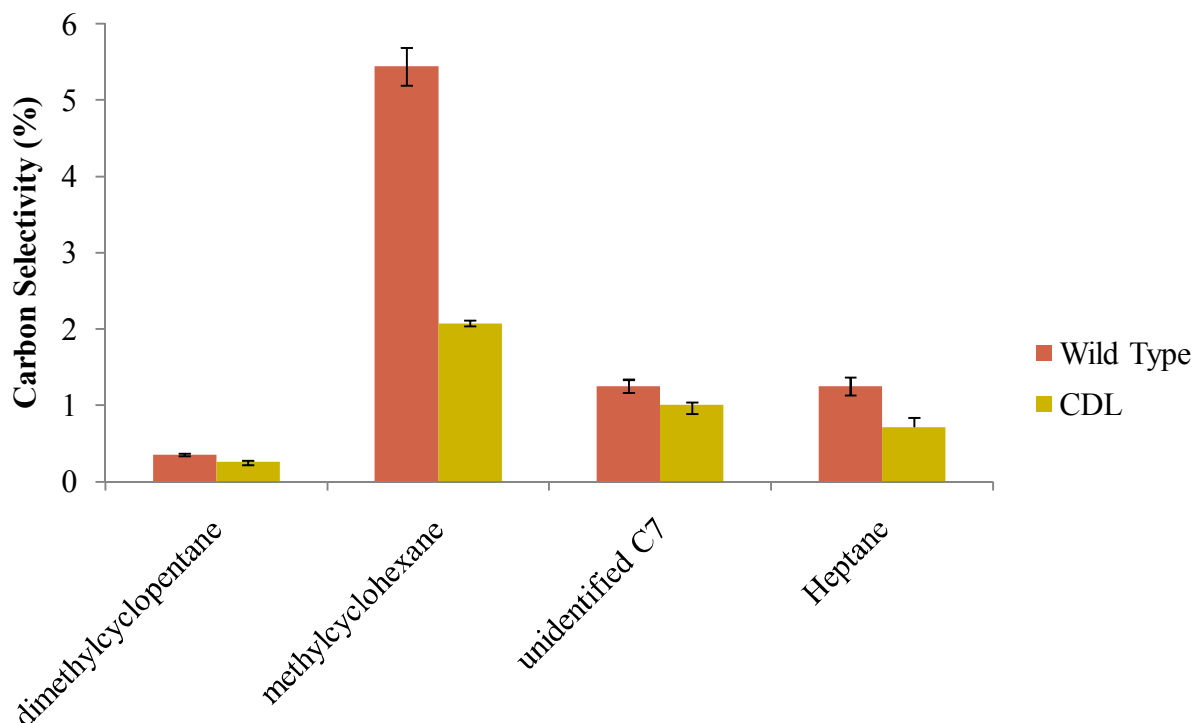


Figure 37: Carbon selectivity to specific C₇ products for HDO of poplar and CDL residue from poplar at 300°C and 20.4 bar H₂

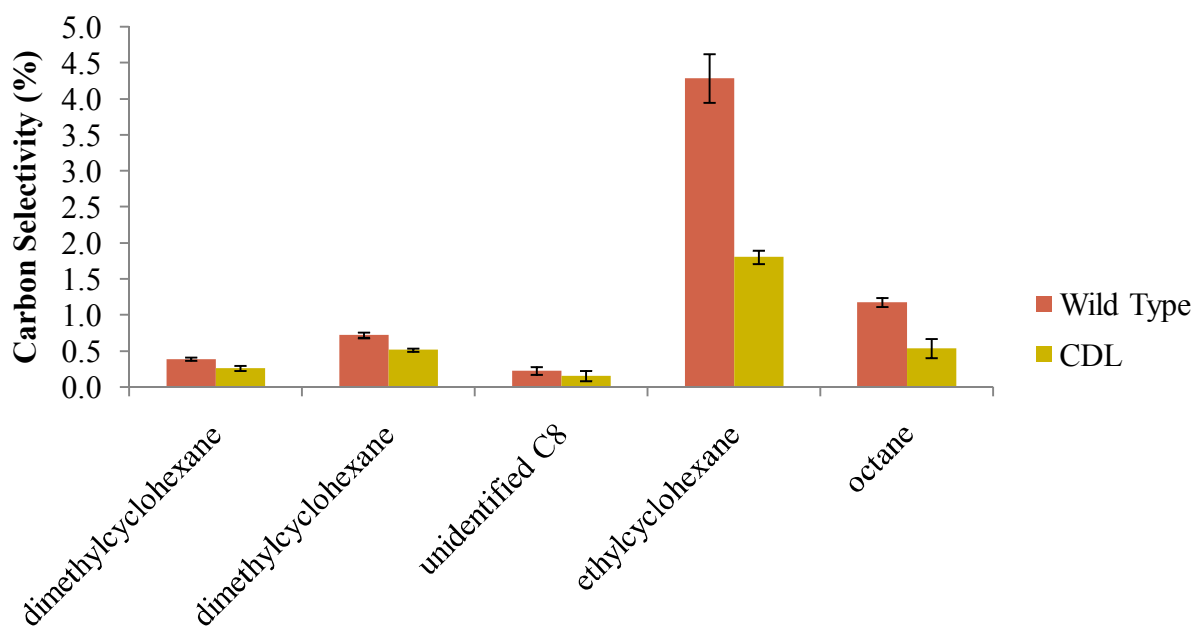


Figure 38: Carbon selectivity to specific C₈ products for HDO of poplar and CDL residue from poplar at 300°C and 20.4 bar H₂

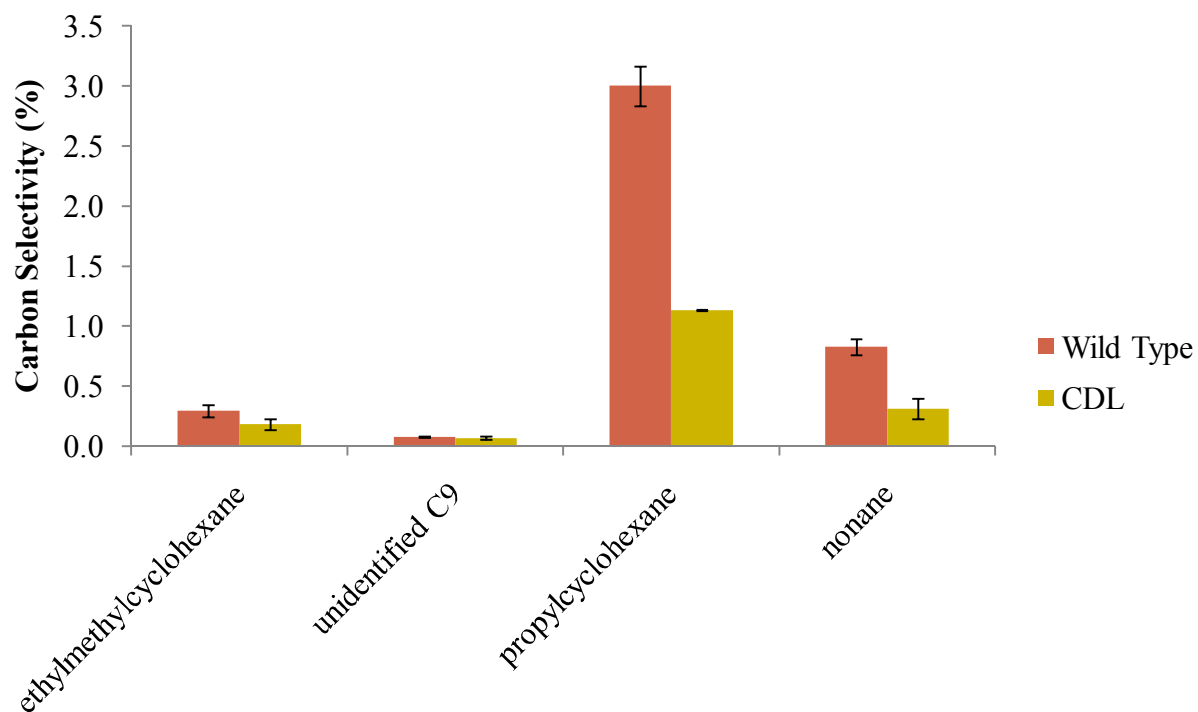


Figure 39: Carbon selectivity to specific C₉ products for HDO of poplar and CDL residue from poplar at 300°C and 20.4 bar H₂

REFERENCES

- [1] R. Agrawal, N.R. Singh, Synergistic routes to liquid fuel for a petroleum-deprived future, *AIChE J.* 55 (2009) 1898–1905. doi:10.1002/aic.11785.
- [2] V.K. Venkatakrishnan, W.N. Delgass, F.H. Ribeiro, R. Agrawal, Oxygen removal from intact biomass to produce liquid fuel range hydrocarbons via fast-hydrolysis and vapor-phase catalytic hydrodeoxygenation, *Green Chem.* 17 (2014) 178–183. doi:10.1039/C4GC01746C.
- [3] Annual Energy Outlook 2015 - Energy Information Administration, (n.d.). <http://www.eia.gov/forecasts/archive/aeo15/> (accessed July 16, 2016).
- [4] S. Singh, S. Jain, V. PS, A.K. Tiwari, M.R. Nouni, J.K. Pandey, S. Goel, Hydrogen: A sustainable fuel for future of the transport sector, *Renew. Sustain. Energy Rev.* 51 (2015) 623–633. doi:10.1016/j.rser.2015.06.040.
- [5] R. Agrawal, N.R. Singh, F.H. Ribeiro, W.N. Delgass, Sustainable fuel for the transportation sector, *Proc. Natl. Acad. Sci.* 104 (2007) 4828–4833. doi:10.1073/pnas.0609921104.
- [6] V.K. Venkatakrishnan, J.C. Degenstein, A.D. Smeltz, W.N. Delgass, R. Agrawal, F.H. Ribeiro, High-pressure fast-pyrolysis, fast-hydrolysis and catalytic hydrodeoxygenation of cellulose: production of liquid fuel from biomass, *Green Chem.* 16 (2014) 792. doi:10.1039/c3gc41558a.
- [7] S. Kim, T.J. Evans, C. Mukarakate, L. Bu, G.T. Beckham, M.R. Nimlos, R.S. Paton, D.J. Robichaud, Furan production from light oxygenates in HZSM-5, *ACS Sustain. Chem. Eng.* (2016). doi:10.1021/acssuschemeng.6b00101.

- [8] N. Mosier, C. Wyman, B. Dale, R. Elander, Y.Y. Lee, M. Holtzapple, M. Ladisch, Features of promising technologies for pretreatment of lignocellulosic biomass, *Bioresour. Technol.* 96 (2005) 673–686. doi:10.1016/j.biortech.2004.06.025.
- [9] P.R. Patwardhan, D.L. Dalluge, B.H. Shanks, R.C. Brown, Distinguishing primary and secondary reactions of cellulose pyrolysis, *Bioresour. Technol.* 102 (2011) 5265–5269. doi:10.1016/j.biortech.2011.02.018.
- [10] P.R. Patwardhan, J.A. Satrio, R.C. Brown, B.H. Shanks, Product distribution from fast pyrolysis of glucose-based carbohydrates, *J. Anal. Appl. Pyrolysis.* 86 (2009) 323–330. doi:10.1016/j.jaap.2009.08.007.
- [11] P.R. Patwardhan, R.C. Brown, B.H. Shanks, Product Distribution from the Fast Pyrolysis of Hemicellulose, *ChemSusChem.* 4 (2011) 636–643. doi:10.1002/cssc.201000425.
- [12] P.R. Patwardhan, R.C. Brown, B.H. Shanks, Understanding the Fast Pyrolysis of Lignin, *ChemSusChem.* 4 (2011) 1629–1636. doi:10.1002/cssc.201100133.
- [13] P. McKendry, Energy production from biomass (part 1): overview of biomass, *Bioresour. Technol.* 83 (2002) 37–46. doi:10.1016/S0960-8524(01)00118-3.
- [14] T. Parsell, S. Yohe, J. Degenstein, T. Jarrell, I. Klein, E. Gencer, B. Hewetson, M. Hurt, J.I. Kim, H. Choudhari, B. Saha, R. Meilan, N. Mosier, F. Ribeiro, W.N. Delgass, C. Chapple, H.I. Kenttämäa, R. Agrawal, M.M. Abu-Omar, A synergistic biorefinery based on catalytic conversion of lignin prior to cellulose starting from lignocellulosic biomass, *Green Chem.* 17 (2015) 1492–1499. doi:10.1039/C4GC01911C.
- [15] S.L. Yohe, H.J. Choudhari, P.J. Dietrich, M.D. Detwiler, C. Akatay, D.D. Mehta, A.R. Dow, H.I. Kenttämäa, W.N. Delgass, R. Agrawal, F.H. Ribeiro, High-Pressure Vapor-Phase Hydrodeoxygenation of Lignin-Derived Oxygenates to Hydrocarbons by a PtMo

- Bimetallic Catalyst: Product Selectivity, Reaction Pathway, and Structural Characterization, (2013).
- [16] H.J. Choudhari, V.K. Venkatakrishnan, I. Smith, I. Klein, M.M. Abu-Omar, W.N. Delgass, R. Agrawal, F.H. Ribeiro, Effect of Hydrogen Pressure during Hydrodeoxygenation of Pyrolysis Products from Biomass and Constituent Polymers, (2014).
- [17] J.D. Wagner, G.R. Lappin, J.R. Zietz, Alcohols, Higher Aliphatic, Synthetic Processes, in: Kirk-Othmer Encycl. Chem. Technol., John Wiley & Sons, Inc., 2000.
<http://onlinelibrary.wiley.com/doi/10.1002/0471238961.1925142023010714.a01/abstract> (accessed July 7, 2016).
- [18] H. Tsuji, F. Yagi, H. Hattori, H. Kita, Self-Condensation of n-Butyraldehyde over Solid Base Catalysts, *J. Catal.* 148 (1994) 759–770. doi:10.1006/jcat.1994.1262.
- [19] J.E. Rekoske, M.A. Barteau, Kinetics, Selectivity, and Deactivation in the Aldol Condensation of Acetaldehyde on Anatase Titanium Dioxide, *Ind. Eng. Chem. Res.* 50 (2011) 41–51. doi:10.1021/ie100394v.
- [20] Z.D. Young, S. Hanspal, R.J. Davis, Aldol Condensation of Acetaldehyde over Titania, Hydroxyapatite and Magnesia, *ACS Catal.* (2016). doi:10.1021/acscatal.6b00264.
- [21] L. Wu, T. Moteki, A.A. Gokhale, D.W. Flaherty, F.D. Toste, Production of Fuels and Chemicals from Biomass: Condensation Reactions and Beyond, *Chem.* (n.d.).
doi:10.1016/j.chempr.2016.05.002.
- [22] T. Moteki, D.W. Flaherty, Mechanistic Insight to C–C Bond Formation and Predictive Models for Cascade Reactions among Alcohols on Ca- and Sr-Hydroxyapatites, *ACS Catal.* (2016). doi:10.1021/acscatal.6b00556.

- [23] J. Li, J. Tai, R.J. Davis, Hydrocarbon oxidation and aldol condensation over basic zeolite catalysts, *Catal. Today*. 116 (2006) 226–233. doi:10.1016/j.cattod.2006.01.032.
- [24] S. Wang, K. Goulas, E. Iglesia, Condensation and esterification reactions of alkanals, alkanones, and alkanols on TiO₂: Elementary steps, site requirements, and synergistic effects of bifunctional strategies, *J. Catal.* 340 (2016) 302–320. doi:10.1016/j.jcat.2016.05.026.
- [25] J.I. Di Cosimo, V.K. Díez, C.R. Apesteguía, Base catalysis for the synthesis of α,β -unsaturated ketones from the vapor-phase aldol condensation of acetone, *Appl. Catal. Gen.* 137 (1996) 149–166. doi:10.1016/0926-860X(95)00289-8.
- [26] W.T. Reichle, Catalytic reactions by thermally activated, synthetic, anionic clay minerals, *J. Catal.* 94 (1985) 547–557. doi:10.1016/0021-9517(85)90219-2.
- [27] S. Malinowski, S. Basinski, Kinetics of aldolic reactions in the gaseous phase on solid catalysts of basic character, *J. Catal.* 2 (1963) 203–207. doi:10.1016/0021-9517(63)90044-7.
- [28] F.M. Scheidt, Vapor-phase aldol condensations over heterogeneous catalysts, *J. Catal.* 3 (1964) 372–378. doi:10.1016/0021-9517(64)90042-9.
- [29] E.L. Kunkes, E.I. Gürbüz, J.A. Dumesic, Vapour-phase C–C coupling reactions of biomass-derived oxygenates over Pd/CeZrO_x catalysts, *J. Catal.* 266 (2009) 236–249. doi:10.1016/j.jcat.2009.06.014.
- [30] E. Dumitriu, N. Bilba, M. Lupascu, A. Azzouz, V. Hulea, G. Cirje, D. Nibou, Vapor-Phase Condensation of Formaldehyde and Acetaldehyde into Acrolein over Zeolites, *J. Catal.* 147 (1994) 133–139. doi:10.1006/jcat.1994.1123.

- [31] J. Dijkmans, W. Schutyser, M. Dusselier, B.F. Sels, Sn β -zeolite catalyzed oxido-reduction cascade chemistry with biomass-derived molecules, *Chem Commun.* 52 (2016) 6712–6715. doi:10.1039/C6CC00199H.
- [32] E. Dumitriu, V. Hulea, N. Bilba, G. Carja, A. Azzouz, Synthesis of acrolein by vapor phase condensation of formaldehyde and acetaldehyde over oxides loaded zeolites, *J. Mol. Catal.* 79 (1993) 175–185. doi:10.1016/0304-5102(93)85100-8.
- [33] M. Ai, Vapor-Phase Aldol Condensation of Formaldehyde with Propionic Acid on Vanadium Pentoxide—Phosphorus Pentoxide, *Appl. Catal.* 36 (1988) 221–230. doi:10.1016/S0166-9834(00)80117-7.
- [34] M.I. Zaki, M.A. Hasan, L. Pasupulety, Surface Reactions of Acetone on Al₂O₃, TiO₂, ZrO₂, and CeO₂: □ IR Spectroscopic Assessment of Impacts of the Surface Acid–Base Properties, *Langmuir.* 17 (2001) 768–774. doi:10.1021/la000976p.
- [35] J.I. Di Cosimo, G. Torres, C.R. Apesteguía, One-Step MIBK Synthesis: A New Process from 2-Propanol, *J. Catal.* 208 (2002) 114–123. doi:10.1006/jcat.2002.3551.
- [36] H.E. Swift, J.E. Bozik, F.E. Massoth, Vapor-phase aldol condensation of n-butyraldehyde using a reduced tin-silica catalyst, *J. Catal.* 15 (1969) 407–416. doi:10.1016/0021-9517(69)90310-8.
- [37] D.G. Hanna, S. Shylesh, Y.-P. Li, S. Krishna, M. Head-Gordon, A.T. Bell, Experimental and Theoretical Study of n-Butanal Self-Condensation over Ti Species Supported on Silica, *ACS Catal.* 4 (2014) 2908–2916. doi:10.1021/cs500704b.
- [38] W. Shen, G.A. Tompsett, R. Xing, W. Curtis Conner Jr., G.W. Huber, Vapor phase butanal self-condensation over unsupported and supported alkaline earth metal oxides, *J. Catal.* 286 (2012) 248–259. doi:10.1016/j.jcat.2011.11.009.

- [39] S. Luo, J.L. Falconer, Aldol condensation of acetaldehyde to form high molecular weight compounds on TiO₂, *Catal. Lett.* 57 (n.d.) 89–93. doi:10.1023/A:1019003817314.
- [40] S. Luo, J.L. Falconer, Acetone and Acetaldehyde Oligomerization on TiO₂ Surfaces, *J. Catal.* 185 (1999) 393–407. doi:10.1006/jcat.1999.2511.
- [41] W.T. Reichle, Pulse microreactor examination of the vapor-phase aldol condensation of acetone, *J. Catal.* 63 (1980) 295–306. doi:10.1016/0021-9517(80)90082-2.
- [42] H. Idriss, K.S. Kim, M.A. Barteau, Carbon–Carbon Bond Formation via Aldolization of Acetaldehyde on Single Crystal and Polycrystalline TiO₂ Surfaces, *J. Catal.* 139 (1993) 119–133. doi:10.1006/jcat.1993.1012.
- [43] M.J.L. Gines, E. Iglesia, Bifunctional Condensation Reactions of Alcohols on Basic Oxides Modified by Copper and Potassium, *J. Catal.* 176 (1998) 155–172. doi:10.1006/jcat.1998.2009.
- [44] J.T. Scanlon, D.E. Willis, Calculation of Flame Ionization Detector Relative Response Factors Using the Effective Carbon Number Concept, *J. Chromatogr. Sci.* 23 (1985) 333–340. doi:10.1093/chromsci/23.8.333.
- [45] K. Tanabe, K. Saito, The conversion of benzaldehyde into benzyl benzoate with alkaline earth metal oxide catalysts, *J. Catal.* 35 (1974) 247–255. doi:10.1016/0021-9517(74)90203-6.
- [46] F. Li, B. Cao, R. Ma, J. Liang, H. Song, H. Song, Performance of Cu/TiO₂-SiO₂ catalysts in hydrogenation of furfural to furfuryl alcohol, *Can. J. Chem. Eng.* (2016) n/a–n/a. doi:10.1002/cjce.22503.

- [47] B.M. Nagaraja, A.H. Padmasri, B. David Raju, K.S. Rama Rao, Vapor phase selective hydrogenation of furfural to furfuryl alcohol over Cu–MgO coprecipitated catalysts, *J. Mol. Catal. Chem.* 265 (2007) 90–97. doi:10.1016/j.molcata.2006.09.037.
- [48] S. Sitthisa, T. Sooknoi, Y. Ma, P.B. Balbuena, D.E. Resasco, Kinetics and mechanism of hydrogenation of furfural on Cu/SiO₂ catalysts, *J. Catal.* 277 (2011) 1–13. doi:10.1016/j.jcat.2010.10.005.
- [49] Z. Wang, Q. Lu, X.-F. Zhu, Y. Zhang, Catalytic Fast Pyrolysis of Cellulose to Prepare Levoglucosenone Using Sulfated Zirconia, *ChemSusChem*. 4 (2011) 79–84. doi:10.1002/cssc.201000210.
- [50] S. Kudo, Z. Zhou, K. Norinaga, J. Hayashi, Efficient levoglucosenone production by catalytic pyrolysis of cellulose mixed with ionic liquid, *Green Chem.* 13 (2011) 3306–3311. doi:10.1039/C1GC15975E.
- [51] Q. Lu, X. Ye, Z. Zhang, C. Dong, Y. Zhang, Catalytic fast pyrolysis of cellulose and biomass to produce levoglucosenone using magnetic SO₄²⁻/TiO₂–Fe₃O₄, *Bioresour. Technol.* 171 (2014) 10–15. doi:10.1016/j.biortech.2014.08.075.
- [52] F.-X. Collard, J. Blin, A review on pyrolysis of biomass constituents: Mechanisms and composition of the products obtained from the conversion of cellulose, hemicelluloses and lignin, *Renew. Sustain. Energy Rev.* 38 (2014) 594–608. doi:10.1016/j.rser.2014.06.013.
- [53] N.D. Bonawitz, C. Chapple, The Genetics of Lignin Biosynthesis: Connecting Genotype to Phenotype, *Annu. Rev. Genet.* 44 (2010) 337–363. doi:10.1146/annurev-genet-102209-163508.

- [54] S.D. Mansfield, K.-Y. Kang, C. Chapple, Designed for deconstruction – poplar trees altered in cell wall lignification improve the efficacy of bioethanol production, *New Phytol.* 194 (2012) 91–101. doi:10.1111/j.1469-8137.2011.04031.x.
- [55] I. Klein, B. Saha, M.M. Abu-Omar, Lignin depolymerization over Ni/C catalyst in methanol, a continuation: effect of substrate and catalyst loading, *Catal. Sci. Technol.* 5 (2015) 3242–3245. doi:10.1039/C5CY00490J.
- [56] T.H. Parsell, B.C. Owen, I. Klein, T.M. Jarrell, C.L. Marcum, L.J. Hauptert, L.M. Amundson, H.I. Kenttämä, F. Ribeiro, J.T. Miller, M.M. Abu-Omar, Cleavage and hydrodeoxygenation (HDO) of C–O bonds relevant to lignin conversion using Pd/Zn synergistic catalysis, *Chem. Sci.* 4 (2013) 806–813. doi:10.1039/C2SC21657D.
- [57] P.R. Patwardhan, J.A. Satrio, R.C. Brown, B.H. Shanks, Influence of inorganic salts on the primary pyrolysis products of cellulose, *Bioresour. Technol.* 101 (2010) 4646–4655. doi:10.1016/j.biortech.2010.01.112.